

GRADIENT FLOW FORMULATION AND SECOND ORDER NUMERICAL METHOD FOR MOTION BY MEAN CURVATURE AND CONTACT LINE DYNAMICS ON ROUGH SURFACE

YUAN GAO

Department of Mathematics, Duke University, Durham, NC

JIAN-GUO LIU

Department of Mathematics and Department of Physics, Duke University, Durham, NC

ABSTRACT. We study the dynamics of a droplet placing on an inclined rough surface, which can be described by gradient flows on a Hilbert manifold. We propose unconditionally stable first/second order numeric schemes to simulate the geometric motion of the droplet described using motion by mean curvature with moving contact lines. The schemes base on (i) explicit moving boundaries, which decouple the dynamics of the contact lines and the capillary surface, (ii) a semi-Lagrangian method on moving grids and (iii) a predictor-corrector method with an inexact nonlinear elliptic solver. To demonstrate the accuracy and long-time validation of the proposed schemes, several challenging computational examples - including breathing droplets, droplets on inhomogeneous rough surfaces and quasi-static Kelvin pendant droplets - are constructed and compared with exact solutions to quasi-static dynamics obtained by desingularized differential-algebraic system of equations (DAEs).

1. INTRODUCTION

The dynamics and equilibrium of a droplet on a substrate are important problems with many practical applications such as coating, painting and printing. The capillary effect, which contributes the leading behaviors of the geometric motion of the droplet, is characterized by the surface tension on interfaces separating two different physical phases. Particularly, the capillary effect greatly affects the dynamics of the contact angle and the contact line of a droplet, where three phases (gas, liquid and solid) meet. Dated back to 1805, YOUNG introduced mean curvature to study the contact angle of a capillary surface and proposed Young's equation for the contact angle, between the capillary surface and the solid substrate, of a static droplet. The geometric motion of a dynamic droplet is more challenging and extensively studied in the literature at the modeling [9, 10, 11, 12], analysis [18, 22, 4, 6, 19, 24, 15, 17], and computations level [38, 32, 30, 33].

E-mail addresses: yuangao@math.duke.edu, jliu@math.duke.edu.

Date: June 6, 2022.

2010 Mathematics Subject Classification. 35R35, 35K93, 65M06, 76T30.

Key words and phrases. Contact angle hysteresis, surface tension, wetting, truncation error estimates.

In this paper, we study the dynamics of a droplet placing on an inclined rough surface using vertical/horizontal graph representation. After deriving the governing equations via gradient flows on a manifold, we propose some unconditionally stable numeric schemes and perform the accuracy check with several challenging examples.

First, we give a gradient flow formulation of the dynamic droplet by regarding the geometric motion of this droplet as a trajectory on a Hilbert manifold with boundary, where the obstacle occurs. Gradient flows on manifolds and the corresponding interpretation of minimizing movement with proper metrics have been the focus of recent researches in both analytic and numerical aspects [3, 27, 1]. This general formulation is also able to describe geometric motions of droplets with topological changes, for instance, splitting and merging. To completely describe the dynamics of the droplet, a free energy including capillary effect and gravitational effect, and a Riemannian metric (dissipation potential) in the gradient flow structure will be specific in different physical settings [9, 2, 12]. For the quasi-static dynamics, i.e. the capillary surface is determined by an elliptic equation, there are many analysis results on the global existence and homogenization problems; see [7, 22, 24, 16] for capillary surface described by harmonic equation and see [4, 5, 8, 17] for capillary surface described by spatial-constant mean curvature equation. We also refer to [2, 17] and the references therein for quantitative/qualitative theory of droplets on rough surface.

Next, we propose some unconditionally stable numerical schemes with second order accuracy for the droplet dynamics described by the motion by mean curvature and the moving contact lines. The unconditionally stable scheme is based on explicit boundary moving, which decouples the dynamics for the contact lines and the capillary surface. The challenging due to moving grids is handled by a semi-Lagrangian method with second order accuracy. To achieve a second order scheme efficiently, we also design a predictor-corrector scheme with inexact nonlinear elliptic solver, which maintains the second order accuracy. There are many other numerical methods proposed for simulating the dynamics of droplets or in general dynamics of multiple interfaces; c.f. the front-tracking method [26], fixed domain method [28], the level set method [40], the phase-field method [20, 23, 35] or the threshold dynamic method [13, 14, 34] and the references therein.

Third, we construct many challenging and important computational examples to demonstrate the validation and efficiency of our numerical schemes. (i) Using a quasi-static solution without gravitational effect, we check the second order accuracy in space and time for our numerical schemes. (ii) We construct a breathing droplet with a closed formula solution, and we use it to show the long-time validation of our numerical schemes. (iii) We use some complicated inclined rough surface such as the classical Utah teapot to demonstrate the contact angle hysteresis of a droplet on inhomogeneous rough surface and the competition between capillary effect and gravitational effect. (iv) Using the horizontal graph representation and a desingularized formula for quasi-static dynamics, we also give some simulations for Kelvin pendant drops with repeated bugles. For recent studies of steady solutions to Kelvin pendant droplet problem, we refer to [30]; see also [32] for simulations of a liquid drop when its volume increases. We also emphasize that there is a rich literature on droplets with different physical effect, such as viscosity effect, Marangoni effect, electromagnetic effect, electronic effect or surfactant effect; see for instance [31, 36, 37, 25].

The rest of this paper is organized as follows. In Section 2, we reformulate the dynamics/quasi-static dynamics of a droplet as a gradient flow on a Hilbert manifold with boundary. The gradient

flow of a specific free energy and the corresponding governing equations for droplets on inclined rough surfaces will be given in Section 2.6. In Section 3, we derive unconditionally stable 1st and 2nd order schemes for droplet dynamics on inclined rough surfaces. The truncation error estimates and pseudo-codes for 1st/2nd order schemes are given in Appendix A and Appendix B respectively. In Section 4, we give some accuracy validations of our schemes compared with the quasi-static solution and demonstrate several challenging examples such as droplet in teapot, breathing droplet and Kelvin pendant droplet.

2. GRADIENT FLOW FORMULATION FOR DYNAMICS OF PARTIALLY WETTING DROPLETS

In this section, we describe the geometric motion of a droplet as a gradient flow with obstacle on a Hilbert manifold. More precisely, we study the motion of a two-dimensional droplet placed on a substrate, which is identified by the area $A := \{(x, y); a \leq x \leq b, 0 \leq y \leq u(x)\}$ with sharp interface. The motion of this droplet is described by a capillary surface $u(x, t) \geq 0$ and partially wetting domain $a(t) \leq x \leq b(t)$ with free boundaries $a(t), b(t)$ (physically known as contact lines). After choosing the configuration states, we will introduce the driving free energy and the dissipation mechanism described by a Riemannian metric, and then we completely determine the motion of the droplet. The dynamics/quasi-static dynamic of droplets with/without volume constraint will be discussed. The extension of gradient flow formulation to a droplet on an inclined rough surface is carried out in Section 2.6. Extension to high-dimensional case is natural for some axial symmetric cases; see Section 4.2.

2.1. Dynamics of a droplet as a gradient flow on manifold: without volume constraint.

Now we describe the geometric motion of the droplet with the configuration states $\eta = \{a, b, u(x)\}$. We use a Hilbert manifold [29] to describe the configuration states

$$(2.1) \quad \mathcal{M} := \{a, b, u(x); u(x) \geq 0, u(x) \in H_0^1(a, b)\}.$$

We use a trajectory on this manifold to describe the dynamics of the droplet. Consider a trajectory $\eta(t) \in \mathcal{M}$ starting from initial state $\eta(0) = \{a(0), b(0), u(x, 0)\} \in \mathcal{M}$,

$$(2.2) \quad \eta(t) = \{a(t), b(t), u(x, t)\} \in \mathcal{M}, \quad t \in [0, T].$$

It is natural to assume the motion of the droplet $\eta(t)$ is modeled by a gradient flow on manifold \mathcal{M} described above. (i) The dynamics is driven by a free energy $\mathcal{F}(\eta)$ on manifold \mathcal{M} ; (ii) The dissipation mechanism of the dynamics is described by a Riemannian metric g_η on the tangent plane $T_\eta\mathcal{M}$, which will be discussed in (2.7) below.

Now we describe the tangent plane $T_\eta\mathcal{M}$. Since the geometric motion has an obstacle condition $u(x, t) \geq 0$, manifold \mathcal{M} has a boundary, i.e. $\{\eta \in \mathcal{M}; u(x) = 0 \text{ for some } x \in (a, b)\}$ (when the droplet has a splitting-type topological change). On the boundary, the tangent plane is not a linear space and has the restriction described below. Following the convention, we will choose the outer normal n of A . Notice

$$(2.3) \quad \frac{du(a(t), t)}{dt} = 0 = \partial_x u(a(t), t)a'(t) + \partial_t u(a(t), t), \quad \frac{du(b(t), t)}{dt} = 0 = \partial_x u(b(t), t)b'(t) + \partial_t u(b(t), t).$$

Denote $v(x, t) := \partial_t u(x, t)$. Then the tangential plane at $\eta(0)$, denoted as $T_\eta \mathcal{M}$ is

$$(2.4) \quad T_\eta \mathcal{M} := \{a', b', v(x) \in H^1(a, b); v(a) = -\partial_x u(a)a', v(b) = -\partial_x u(b)b', v(x) + u(x) \geq 0\}.$$

Here a', b' are the horizontal velocity at the contact ending points (physically also known as the contact line speeds) and $v(x)$, $x \in [a, b]$ is the vertical velocity. The last inequality in the definition of $T_\eta \mathcal{M}$ in (2.4) is only effective for η on the boundary of the manifold \mathcal{M} , i.e. where the obstacle occurs.

Define the contact angles (inside the droplet A) as

$$(2.5) \quad \tan \theta_a := \partial_x u(a), \quad \tan \theta_b := -\partial_x u(b);$$

see Fig 1 (a). Then the physical meaning of the constraint in (2.4) is naturally from the fact that the contact angles are proportional to the quotient of the vertical velocity and the horizontal velocity, i.e.

$$(2.6) \quad \tan \theta_a = \partial_x u(a) = \frac{v(a)}{-a'}, \quad \tan \theta_b = -\partial_x u(b) = \frac{v(b)}{b'}.$$

Next, one need to propose some dynamic boundary conditions describing the relations between the contact line speeds a', b' and the contact angles θ_a, θ_b . Under the smoothness assumption for the relation between the contact angle and the contact line speed, linearized around the equilibrium, DAVIS [9] obtained the linear relation between the perturbed contact line speed and the perturbed contact angle. This is consistent with Onsager's quadratic dissipation potential (see also DOI [37]), which leads to the first two terms in the Riemannian metric introduced in (2.7) below; see [22] for both L^1 and L^2 Riemannian metrics. We also refer to [2] for a different L^1 metric for the contact line speed, which gives a rate independent gradient flow [27].

To describe the dissipation mechanism of the dynamics, we introduce the a Riemannian metric g_η . For any $q_1 = (a'_1, b'_1, v_1(x)), q_2 = (a'_2, b'_2, v_2(x)) \in T_\eta \mathcal{M}$, define the Riemannian metric g_η on $T_\eta \mathcal{M} \times T_\eta \mathcal{M}$ as

$$(2.7) \quad g_\eta(q_1, q_2) := a'_1 a'_2 + b'_1 b'_2 + \beta \int_a^b v_1(x) v_2(x) \frac{dx}{\sqrt{1 + u_x^2}},$$

where $\beta > 0$ indicates the capillary relaxation time on the capillary surface.

We consider the energy functional

$$(2.8) \quad \mathcal{F}(\eta) = \mathcal{F}(a, b, u) = \int_a^b G(x, u, \partial_x u(x)) dx.$$

Particularly, one can consider three typical free energies: (i) Dirichlet energy $G(x, u, u_x) = \frac{1}{2} \partial_x u^2 + \sigma$, where σ is a constant; c.f. [7, 24, 16, 37]; (ii) Area functional $G(x, u, u_x) = \sqrt{1 + (\partial_x u)^2} + \sigma$; c.f. [4, 5, 17], as a consequence, the choice of the last term in g_η gives the mean curvature flow; c.f. [21]; (iii) free energy for droplets on inclined rough surface; see (2.35) below.

We now derive the gradient flow of $\mathcal{F}(\eta)$ on manifold \mathcal{M} with respect to the Riemannian metric g_η . For an arbitrary trajectory $\tilde{\eta}(s) = \{\tilde{a}(s), b(s), \tilde{u}(x, s)\}$ (physically known as a virtual displacement) passing $\tilde{\eta}(t) = \eta(t)$ with tangent direction $q := \tilde{\eta}'(t) = \{\tilde{a}', \tilde{b}', \tilde{v}(x)\} \in T_{\eta(t)} \mathcal{M}$, we know

$$(2.9) \quad \tilde{v}(a) = -\partial_x u|_a \tilde{a}', \quad \tilde{v}(b) = -\partial_x u|_b \tilde{b}'.$$

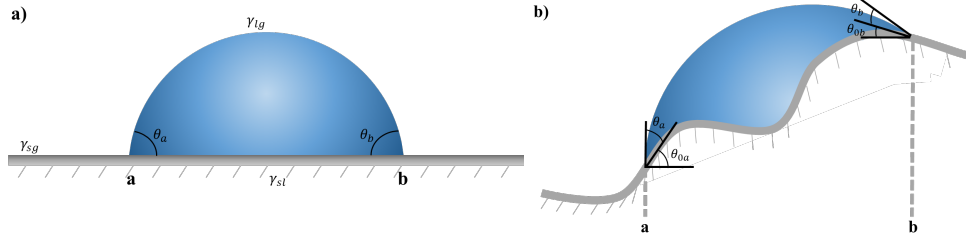


FIGURE 1. (a) Illustration of contact angles θ_a, θ_b ; (b) Illustration of contact angles θ_a, θ_b and the local slopes of the rough surface θ_{0a}, θ_{0b} .

the gradient flow on manifold \mathcal{M} can be formulated by

$$(2.10) \quad g_{\eta(t)}(q, \eta'(t)) + \frac{d}{ds} \Big|_{s=t^+} \mathcal{F}(\tilde{\eta}(s)) = 0$$

for any $q \in T_{\eta(t)}\mathcal{M}$, i.e.,

$$(2.11) \quad g_{\eta(t)}(q, \eta'(t)) + \frac{d}{ds} \Big|_{s=t^+} \int_{\tilde{a}(s)}^{\tilde{b}(s)} G(x, \tilde{u}(x, s), \partial_x \tilde{u}(x, s)) dx = 0.$$

From (2.9),

$$(2.12) \quad \begin{aligned} & \frac{d}{ds} \Big|_{s=t^+} \int_{\tilde{a}(s)}^{\tilde{b}(s)} G(x, \tilde{u}(x, s), \partial_x \tilde{u}(x, s)) dx \\ &= G|_b \tilde{b}' - G|_a \tilde{a}' + \int_a^b \partial_u G \tilde{v} + \partial_{u_x} G \partial_x \tilde{v} dx \\ &= G|_b \tilde{b}' - G|_a \tilde{a}' + \int_a^b (\partial_u G - \frac{d}{dx} (\partial_{u_x} G)) \tilde{v} dx + \tilde{v} \partial_{u_x} G|_a^b \\ &= (G - \partial_x u \partial_{u_x} G)|_b \tilde{b}' - (G - \partial_x u \partial_{u_x} G)|_a \tilde{a}' + \int_a^b (\partial_u G - \frac{d}{dx} (\partial_{u_x} G)) \tilde{v} dx. \end{aligned}$$

Notice also from the Riemannian metric $g_{\eta(t)}$,

$$(2.13) \quad g_{\eta(t)}(q, \eta'(t)) = \tilde{a}' a'(t) + \tilde{b}' b'(t) + \beta \int_{a(t)}^{b(t)} \tilde{v} \frac{\partial_t u(x, t)}{\sqrt{1 + (\partial_x u)^2}} dx,$$

where $\frac{\partial_t u(x, t)}{\sqrt{1 + (\partial_x u)^2}}$ is the normal velocity in the direction of the outer normal.

Now we derive the governing equations by taking different $q \in T_{\eta(t)}\mathcal{M}$. First, taking $q = \{\tilde{a}', 0, 0\} \in T_{\eta(t)}\mathcal{M}$, from (2.11), we have the equation at the endpoint a ,

$$(2.14) \quad a'(t) = (G - \partial_x u \partial_{u_x} G)|_{a(t)}.$$

Similarly, we can derive the equation at the endpoint b . Thus the governing equations for $u(\cdot, t) \in H_0^1(a(t), b(t))$ are

$$(2.15) \quad \begin{aligned} & a'(t) = (G - \partial_x u \partial_{u_x} G)|_{a(t)}, \\ & b'(t) = -(G - \partial_x u \partial_{u_x} G)|_{b(t)}, \\ & \int_{a(t)}^{b(t)} \left[\beta \frac{\partial_t u(x, t)}{\sqrt{1 + (\partial_x u)^2}} + (\partial_u G - \frac{d}{dx} (\partial_{u_x} G)) \right] v dx = 0, \quad \forall v \in H_0^1(a, b), v(x) + u(x, t) \geq 0. \end{aligned}$$

2.2. Gradient flow on a manifold for a Obstacle Problem: with volume constraint. In this section, we consider a gradient flow with volume constraint. Recall (2.1), (2.4) and denote the volume of the droplet as V . To ensure the volume preserving condition $\int_{a(t)}^{b(t)} u \, dx = V$, $t \in [0, T]$, we consider the gradient flow of extended free energy $\mathcal{F}(\eta, \lambda)$ on manifold $\mathcal{M} \times \mathbb{R}$ for $\eta(t) \in \mathcal{M}$ and a Lagrange multiplier $\lambda(t)$

$$(2.16) \quad \mathcal{F}(\eta(t), \lambda(t)) = \mathcal{F}(\eta(t)) - \lambda(t) \left(\int_{a(t)}^{b(t)} u(t) \, dx - V \right).$$

Then the gradient flow of $\mathcal{F}(\eta, \lambda)$ with respect to Riemannian metric g_η defined in (2.7) is

$$(2.17) \quad -g_{\eta(t)}(q, \eta'(t)) = \frac{d}{ds} \Big|_{s=t^+} \mathcal{F}(\tilde{\eta}(s), \tilde{\lambda}(s)) = \frac{d}{ds} \Big|_{s=t^+} \mathcal{F}(\tilde{\eta}(s)) - \langle v, \lambda(t) \rangle - \tilde{\lambda}'(t) \left(\int_{a(t)}^{b(t)} u \, dx - V \right).$$

Therefore the governing equations for $u(\cdot, t) \in H_0^1(a(t), b(t))$ and $\lambda(t)$ are

$$(2.18) \quad a'(t) = (G - \partial_x u \partial_{u_x} G) \Big|_{a(t)},$$

$$(2.19) \quad b'(t) = -(G - \partial_x u \partial_{u_x} G) \Big|_{b(t)},$$

$$(2.20) \quad \int_{a(t)}^{b(t)} \left[\beta \frac{\partial_t u(x, t)}{\sqrt{1 + (\partial_x u)^2}} + \partial_u G - \frac{d}{dx} (\partial_{u_x} G) - \lambda(t) \right] v \, dx = 0,$$

$$(2.21) \quad \forall v \in H_0^1(a, b), v(x) + u(x, t) \geq 0,$$

$$(2.22) \quad \int_{a(t)}^{b(t)} u(x, t) \, dx = V.$$

2.3. Gradient flow for a single droplet: without merging and splitting. The variational inequality formula above are able to describe the merging and splitting of several drops. However, how many parts the droplet will end up is unknown. When the droplet is separated into two parts, and ideally the generated contact line speed has the same formula with (2.18) and (2.19), we can treat them separately. Existence of global weak solutions including topological changes (splitting and merging) is studied in [22] using a continuum limit of a time discretization. We call a separated droplet as a single sessile drop if $u(x, t) > 0$ for $x \in (a(t), b(t))$ with the gravity downwards, i.e. $g > 0$. Another scenario is when a light drop is in a heavy fluid, the drop experience buoyancy due to gravity. In this case, we call a separated droplet as a single pendant drop if $u(x, t) > 0$ for $x \in (a(t), b(t))$ with the gravity upwards, i.e. $g < 0$. Another equivalent problem is a drop pendant on ceiling with $u < 0$ for $x \in (a(t), b(t))$ and $g > 0$. In the remaining paper, we only consider nonnegative solutions. For those single sessile/pendant drop cases, the variational inequalities become variational equalities and the weak formulations can be equivalently converted to a strong PDE formulations. Therefore the governing equations without volume constrain (2.15) become

$$(2.23) \quad \begin{aligned} & \beta \frac{\partial_t u(x, t)}{\sqrt{1 + (\partial_x u)^2}} + \partial_u G - \frac{d}{dx} (\partial_{u_x} G) = 0, \quad a(t) < x < b(t), \\ & u(a(t), t) = u(b(t), t) = 0, \\ & a'(t) = (G - \partial_x u \partial_{u_x} G) \Big|_{a(t)}, \\ & b'(t) = -(G - \partial_x u \partial_{u_x} G) \Big|_{b(t)}, \end{aligned}$$

and the governing equations with volume constraint (2.18)-(2.22) become

$$\begin{aligned}
(2.24) \quad & \beta \frac{\partial_t u(x, t)}{\sqrt{1 + (\partial_x u)^2}} + \partial_u G - \frac{d}{dx}(\partial_{u_x} G) - \lambda(t) = 0, \quad a(t) < x < b(t), \\
& u(a(t), t) = u(b(t), t) = 0, \\
& a'(t) = (G - \partial_x u \partial_{u_x} G)|_{a(t)}, \\
& b'(t) = -(G - \partial_x u \partial_{u_x} G)|_{b(t)}, \\
& \int_{a(t)}^{b(t)} u(x, t) dx = V,
\end{aligned}$$

where V is the initial volume of the droplet.

2.4. Gradient flow for a single droplet with quasi-static dynamics. If we consider the gradient flow in the quasi-static setting, i.e. $\beta = 0$, we can regard $u(x, t)$ as being driven by $a(t), b(t)$. In other words, we consider $\{a(t), b(t), u(x, t)\}$ with $u(x, t)$ as the solution to

$$\begin{aligned}
(2.25) \quad & \partial_u G - \frac{d}{dx}(\partial_{u_x} G) = 0, \quad a(t) < x < b(t), \\
& u(a(t), t) = u(b(t), t) = 0.
\end{aligned}$$

This gives a reduced manifold $\mathbb{R}^2 = \{a, b\}$. Correspondingly, we have the quasi-static trajectory $\eta_{qs}(t) := (a(t), b(t))$, the quasi-static tangent plane $T_{\eta_{qs}}$ and the quasi-static free energy

$$(2.26) \quad \mathcal{F}_{qs}(a(t), b(t)) := \mathcal{F}((a(t), b(t), u(x, t))).$$

With the quasi-static metrics $g_{\eta_r}(\eta'_r, \tilde{\eta}'_r) = a' \tilde{a}' + b' \tilde{b}'$, we have the gradient flow for quasi-static dynamics

$$\begin{aligned}
(2.27) \quad & \frac{d}{ds} \Big|_{s=t} \mathcal{F}(\tilde{\eta}(s)) = \frac{d}{ds} \Big|_{s=t} \mathcal{F}_{qs}(\tilde{\eta}_{qs}(s)) = \frac{\partial \mathcal{F}_{qs}}{\partial a} \tilde{a}'(t) + \frac{\partial \mathcal{F}_{qs}}{\partial b} \tilde{b}'(t) \\
& = -g_{\eta_{qs}}(\eta'_r, \tilde{\eta}'_{qs}) = -a'(t) \tilde{a}'(t) - b'(t) \tilde{b}'(t).
\end{aligned}$$

Then by the calculation in (2.12), we have the gradient flow for $a(t), b(t)$

$$\begin{aligned}
(2.28) \quad & a'(t) = -\frac{\partial \mathcal{F}_{qs}}{\partial a} = (G - \partial_x u \partial_{u_x} G)|_{a(t)}, \\
& b'(t) = -\frac{\partial \mathcal{F}_{qs}}{\partial b} = -(G - \partial_x u \partial_{u_x} G)|_{b(t)}.
\end{aligned}$$

Notice the right hand sides depend on u which is solved by the nonlinear elliptic equation (2.25). Combing the ODE (2.28) with the elliptic equation (2.25) gives a complete description of the quasi-static dynamics of the droplet. After spatial discretization, the resulted system is known as a differential-algebraic system of equations (DAEs); see detailed description in Section 4.1.1.

2.5. Free energy for the droplet and Young's angle. To give a specific free energy, we will follow the same notations and terminologies in the classical book of De Gennes [11]. To consider the interactions between the three phases of materials: gas, liquid, and solid, denote γ_{sl} (γ_{sg}, γ_{lg} resp.) as the interfacial surface energy density between solid-liquid phases (solid-gas, liquid-gas resp.). $\gamma_{sl}, \gamma_{sg}, \gamma_{lg} > 0$ are also known as the surface tension coefficients. Surface tension contributes the leading effect to the dynamics and equilibrium of the droplet. Surface energy between liquid

and gas is the excess energy due to the one half lower coordination number (in the mean field approximation) of molecules at the surface compared with those sitting in the liquid bulk (DOI [12]). Besides gravity, we neglect other forces, such as viscosity effect, Marangoni effect (solutocapillary effect and thermocapillary effect), electromagnetic effect, evaporation and condensation, etc. To count the total area of the capillary surface (with surface tension γ_{lg}) and the area of the contact domain of the droplet (with the relative surface tension $\gamma_{sl} - \gamma_{sg}$), we take the total free energy of the droplet as

$$(2.29) \quad \mathcal{F}(\eta(t)) = \gamma_{lg} \int_{a(t)}^{b(t)} \sqrt{1 + (\partial_x u)^2} dx + (\gamma_{sl} - \gamma_{sg}) \int_{a(t)}^{b(t)} dx + \rho g \int_{a(t)}^{b(t)} \frac{u^2}{2} dx,$$

where ρ is the density of the liquid, g is the gravitational acceleration. The competition between the three surface tension coefficients will in the end determine the steady shape of the droplet. Let the density of gas outside the droplet is $\rho_0 = 0$. We denote the capillary coefficient as $\kappa := \frac{\rho g}{\gamma_{lg}}$ and the capillary length as $L_c := \frac{1}{\sqrt{\kappa}}$. For a droplet with volume V , its equivalent length (characteristic length) L is defined as $V = \frac{4\pi}{3} L^3$ in 3D and $V = \pi L^2$ in 2D. The bond number $\text{Bo} := (\frac{L}{L_c})^2 = \kappa L^2$ shall be small enough to observe the capillary effect [11]. Notice for simplicity in presentations of the governing equations, we allow $\kappa < 0$ in the case of pendant droplet. Hence when $\kappa < 0$, the capillary length is $L_c = \frac{1}{\sqrt{|\kappa|}}$ and the bond number is $\text{Bo} = (\frac{L}{L_c})^2 = |\kappa| L^2$.

By Young's equation [39], the equilibrium contact angle θ_Y is determined by the Young's angle condition

$$(2.30) \quad \cos \theta_Y = \frac{\gamma_{sg} - \gamma_{sl}}{\gamma_{lg}}.$$

Adhesive forces between the liquid and the solid cause the liquid drop to spread across the surface (called a partially wetting liquid on a hydrophilic surface), while cohesive forces within the liquid cause the drop to ball up and avoid contact with the surface (called dewetting or non-wetting liquid on a hydrophobic surface).

From Young's angle condition (2.30) the partially wetting liquid case (hydrophilic surface) corresponds to

$$\sigma := \frac{\gamma_{sl} - \gamma_{sg}}{\gamma_{lg}} = -\cos \theta_Y \leq 0, \quad 0 < \theta_Y \leq \frac{\pi}{2},$$

where σ is called relative adhesion coefficient between the liquid and the solid. In this case, the relative adhesion coefficient $-1 < \sigma \leq 0$. On the other hand, the non-wetting liquid case (hydrophobic surface) corresponds to

$$\sigma = \frac{\gamma_{sl} - \gamma_{sg}}{\gamma_{lg}} = -\cos \theta_Y \geq 0, \quad \frac{\pi}{2} \leq \theta_Y < \pi.$$

In this case, the relative adhesion coefficient $0 \leq \sigma < 1$. The case $\theta_Y = 0$, $\sigma = -1$ is called completely wetting. For simplicity, we assume $\gamma_{lg} = 1$ in this paper.

2.6. Gradient flow for a single droplet on a rough and inclined surface. In this section, with some modifications for the free energy and the Riemannian metric, we turn to describe the gradient flow and the governing equations for a single droplet on a rough and inclined surface. Given a rough solid surface described by a graph function $w(x)$, the droplet is then described by

$$(2.31) \quad A := \{(x, y); a \leq x \leq b, w(x) \leq y \leq u(x) + w(x)\}.$$

Here we follow the convention for studying droplets on an inclined surface and use the Cartesian coordinate system built on an inclined plane with effective inclined angle θ_0 such that $-\frac{\pi}{2} < \theta_0 < \frac{\pi}{2}$, i.e. $\tan \theta_0 x$ is the new x -axis we choose.

The motion of this droplet is described by the relative height function (capillary surface) $u(x, t) \geq 0$ and partially wetting domain $a(t) \leq x \leq b(t)$ with free boundaries $a(t), b(t)$. Consider the manifold

$$(2.32) \quad \mathcal{M} := \{a, b, u(x); u(x) \geq 0, u(x) \in H_0^1(a, b)\}.$$

Then the tangential plane at $\eta(0)$, denoted as $T_\eta \mathcal{M}$ is

$$(2.33) \quad T_\eta \mathcal{M} := \{a', b', v(x) \in H^1(a, b); v(x) + u(x) \geq 0, v(a) = -\partial_x u(a) a', v(b) = -\partial_x u(b) b'\}.$$

Define the Riemannian metric $g_{\eta(t)}$ for the rough surface

$$(2.34) \quad g_{\eta(t)}(q, \eta'(t)) = \tilde{a}' a'(t) + \tilde{b}' b'(t) + \beta \int_{a(t)}^{b(t)} \tilde{v} \frac{\partial_t u(x, t)}{\sqrt{1 + (\partial_x(u+w))^2}} dx,$$

where $q = (\tilde{a}', \tilde{b}', \tilde{v}(x))$ and $\frac{\partial_t u(x, t)}{\sqrt{1 + (\partial_x(u+w))^2}}$ is the normal velocity along the outer normal direction.

Now we consider the energy functional associated with the rough surface

$$(2.35) \quad \begin{aligned} \mathcal{F}(\eta(t)) = & \gamma_l g \int_{a(t)}^{b(t)} \sqrt{1 + (\partial_x(u+w))^2} dx + (\gamma_{sl} - \gamma_{sg}) \int_{a(t)}^{b(t)} \sqrt{1 + (\partial_x w)^2} dx \\ & + \rho g \int_{a(t)}^{b(t)} \int_{h_0}^{u+h_0} (y \cos \theta_0 + x \sin \theta_0) dy dx, \end{aligned}$$

where ρ is the density of the liquid, g is the gravitational acceleration. In the inclined case, for a droplet with volume V in 2D, the effective bond number is

$$(2.36) \quad Bo := \left(\frac{L}{L_c}\right)^2 \cos \theta_0 = \kappa L^2 \cos \theta_0.$$

To ensure the volume preserving condition $\int_{a(t)}^{b(t)} u dx =: V$, we consider the gradient flow of an extended free energy $\mathcal{F}(\eta, \lambda)$ on manifold $\mathcal{M} \times \mathbb{R}$ for $\eta(t) \in \mathcal{M}$ and the Lagrange multiplier $\lambda(t)$

$$(2.37) \quad \mathcal{F}(\eta(t), \lambda(t)) = \mathcal{F}(\eta(t)) - \lambda(t) \left(\int_{a(t)}^{b(t)} u(t) dx - V \right).$$

Then the gradient flow associated with $\mathcal{F}(\eta, \lambda)$ with respect to Riemannian metric g_η defined in (2.7) is

$$(2.38) \quad -g_\eta(q, \eta'(t)) = \frac{d}{ds} \Big|_{s=t^+} \mathcal{F}(\tilde{\eta}(s), \tilde{\lambda}(s)) = \frac{d}{ds} \Big|_{s=t^+} \mathcal{F}(\tilde{\eta}(s)) - \langle v, \lambda(t) \rangle - \tilde{\lambda}'(t) \left(\int_{a(t)}^{b(t)} u dx - V \right).$$

By energy functional (2.35), and same calculations as that for (2.18)-(2.21),

$$G = \sqrt{1 + (\partial_x(u+w))^2} + \sigma \sqrt{1 + (\partial_x w)^2} + \kappa \left(\frac{u^2 \cos \theta_0}{2} + \cos \theta_0 u w + x \sin \theta_0 u \right)$$

with

$$\partial_u G = \kappa((u+w) \cos \theta_0 + x \sin \theta_0), \quad \partial_{u_x} G = \frac{\partial_x(u+w)}{\sqrt{1 + (\partial_x(u+w))^2}}.$$

For simplicity, we denote $h(x, t) := u(x, t) + w(x)$, then the governing equations for a single droplet become

$$\begin{aligned}
 \beta \frac{\partial_t h(x, t)}{\sqrt{1 + (\partial_x h)^2}} &= \frac{\partial}{\partial x} \left(\frac{\partial_x h}{\sqrt{1 + (\partial_x h)^2}} \right) - \kappa(h \cos \theta_0 + x \sin \theta_0) + \lambda(t), \quad x \in (a(t), b(t)), \\
 u(a(t), t) &= u(b(t), t) = 0, \\
 (2.39) \quad a'(t) &= \sigma \sqrt{1 + (\partial_x w)^2} + \frac{1 + \partial_x h \partial_x w}{\sqrt{1 + (\partial_x h)^2}} = \frac{1}{\cos \theta_{0a}} (\cos \theta_a - \cos \theta_Y), \quad x = a(t), \\
 b'(t) &= -\sigma \sqrt{1 + (\partial_x w)^2} - \frac{1 + \partial_x h \partial_x w}{\sqrt{1 + (\partial_x h)^2}} = -\frac{1}{\cos \theta_{0b}} (\cos \theta_b - \cos \theta_Y), \quad x = b(t), \\
 &\int_{a(t)}^{b(t)} u(x, t) dx = V,
 \end{aligned}$$

where the two angles are defined as $\partial_x w|_a = \tan \theta_{0a}$, $\partial_x h|_a = \tan(\theta_{0a} + \theta_a)$ and $\partial_x w|_b = -\tan \theta_{0b}$ and $\partial_x h|_b = -\tan(\theta_{0b} + \theta_b)$; see Fig 1 (b). It is easy to check the steady state $a'(t) = b'(t) = 0$ recovers Young's angle condition.

Remark 1. For $w(x) = 0$, i.e. the surface is a perfect inclined plane with angle θ_0 , the derivation above recovers the classical model for capillary droplets on an inclined surface.

Remark 2. We remark the first equation in (2.39) with the free parameter $\lambda(t)$ is translation invariant for x to $x + x_0$. At the equilibrium, the right hand side in the first equation is exactly the hydrostatic balance

$$(2.40) \quad -(p + \rho gh) = \gamma_l g \frac{\partial}{\partial x} \left(\frac{\partial_x h}{\sqrt{1 + (\partial_x h)^2}} \right) - \gamma_l g \kappa (h \cos \theta_0 + x \sin \theta_0) = \text{const} = -\gamma_l g \lambda,$$

where we have chosen by convention the pressure outside of the drop to be zero and inside $p = -\gamma_l g \frac{\partial}{\partial x} \left(\frac{\partial_x h}{\sqrt{1 + (\partial_x h)^2}} \right)$ due to the force balance on the capillary surface.

3. NUMERICAL SCHEMES FOR DROPLETS DYNAMICS ON A ROUGH AND INCLINED SURFACE

In this section, we consider a droplet (described by a vertical graph function) on a rough and inclined surface in the partially wetting case, i.e. the relative adhesion coefficient $-1 < \sigma \leq 0$. Notice the dynamics for the moving boundary $a(t), b(t)$ in (2.39) leads to a uniform upper/lower bound, we have an unconditionally stable explicit scheme for the time stepping of moving boundary; see Remark 3. This explicit discretization decouples the computations for the moving boundary $a(t), b(t)$ and capillary surface $u(x, t)$. To achieve a second order scheme in time and space, we should particularly take care of the following issues. First, due to the moving grids $x^n \in (a^n, b^n)$ for each time step n , one need to map $h^n(x^n)$, $x^n \in (a^n, b^n)$ to $h^{n*}(x^{n+1})$, $x^{n+1} \in (a^{n+1}, b^{n+1})$ based on a semi-Lagrangian method upto second order accuracy. Second, to achieve a second order scheme efficiently, we design a predictor-corrector scheme with inexact nonlinear elliptic solver, which maintains the overall second order accuracy. Third, the effects from the inclined rough substrate and the volume constraint will be included. We will derive the first order scheme and give its truncation error in Section 3.1. Then we derive the second order scheme and give its

truncation error in Section 3.2. The proofs for truncation error estimates will be left to Appendix A. Before we present the schemes, we list some key notations below in Table 1.

TABLE 1. Commonly used notations in this paper.

Symbols	Meaning
$t^n = n\Delta t$ $a(t^n), b(t^n)$ a^n, b^n $\tilde{a}^{n+1}, \tilde{b}^{n+1}$	Time Grids PDE moving boundary at t^n Numerical moving boundary at t^n Predictor numerical moving boundary at t^{n+1}
$x^n \in [a(t^n), b(t^n)]$ $x^n \in [a^n, b^n]$ $x_j^n = a^n + j\tau^n, \tau^n = \frac{b^n - a^n}{N}$ $\tilde{x}^{n+1} \in [\tilde{a}^{n+1}, \tilde{b}^{n+1}]$ $\tilde{x}_j^{n+1} = \tilde{a}^{n+1} + j\tilde{\tau}^{n+1}, \tilde{\tau}^{n+1} = \frac{\tilde{b}^{n+1} - \tilde{a}^{n+1}}{N}$	PDE spatial variable at t^n Numerical spatial variable at t^n Moving spatial grids at t^n Predictor variable at t^{n+1} Predictor moving grids at t^{n+1}
$h(x^n, t^n), u(x_j^n, t^n)$ for $x^n \in [a(t^n), b(t^n)]$ $h^n(x^n), u_j^n$ for $x^n \in [a^n, b^n]$ $h^*(x^{n+1}, t^n)$ $h^{n*}(x^{n+1}), h_j^{n*}$	PDE solution at t^n Numerical solution at t^n Rescaled PDE solution at t^n Numerical rescaled solution at t^n
$\tilde{h}(\tilde{x}^{n+1}, t^{n+1}), \tilde{h}(\tilde{x}_j^{n+1}, t^{n+1})$ $\tilde{h}^{n+1}(\tilde{x}^{n+1}), \tilde{h}_j^{n+1}$ $\tilde{h}^{n*}(x^{n+1}), \tilde{h}_j^{n*}$	Predictor PDE solution at t^{n+1} Predictor numerical solution at t^{n+1} Intermedia numerical rescaled solution from predictor

3.1. First order unconditionally stable scheme based on explicit boundary moving and semi-implicit motion by mean curvature.

3.1.1. *First order scheme based on explicit boundary moving and semi-implicit motion by mean curvature.* Now we design a numerical algorithm for the motion by mean curvature in (2.39).

Let $t^n = n\Delta t$, $n = 0, 1, 2, \dots$ with time step Δt . We approximate $a(t^n), b(t^n)$ by a^n, b^n respectively. With some proper spatial discretizations (such as finite difference, finite element, spectral approximation), we approximate $h(x^n, t^n)$ by $h^n(x^n)$ for $x^n \in (a^n, b^n)$. We approximate $\lambda(t^n)$ by λ^n . We propose the following three-step algorithm for updating a^n, b^n, h^n, λ^n from n to $n+1$.

Step 1. Compute the one-side approximated derivative of h^n at b^n and a^n , denoted as $(\partial_x h^n)_N$ and $(\partial_x h^n)_0$. Then by the dynamic boundary condition in (2.39), we update a^{n+1}, b^{n+1} using

$$(3.1) \quad \begin{aligned} \frac{a^{n+1} - a^n}{\Delta t} &= \sigma \sqrt{1 + (\partial_x w)_0^2} + \frac{1 + (\partial_x h^n)_0 (\partial_x w)_0}{\sqrt{1 + (\partial_x h^n)_0^2}}, \\ \frac{b^{n+1} - b^n}{\Delta t} &= -\sigma \sqrt{1 + (\partial_x w)_N^2} - \frac{1 + (\partial_x h^n)_N (\partial_x w)_N}{\sqrt{1 + (\partial_x h^n)_N^2}}. \end{aligned}$$

Step 2. Rescale h^n from $[a^n, b^n]$ to $[a^{n+1}, b^{n+1}]$ with $O(\Delta t^2)$ accuracy using a semi-Lagrangian discretization. For $x^{n+1} \in [a^{n+1}, b^{n+1}]$, denote the map from moving grids at t^{n+1} to t^n as

$$(3.2) \quad x^n := a^n + \frac{b^n - a^n}{b^{n+1} - a^{n+1}} (x^{n+1} - a^{n+1}) \in [a^n, b^n].$$

Define the rescaled solution for h^n as

$$(3.3) \quad h^{n*}(x^{n+1}) := h^n(x^n) + \partial_x h^n(x^n)(x^{n+1} - x^n).$$

It is easy to verify by the Taylor expansion $h^{n*}(x^{n+1}) = h^n(x^{n+1}) + O(|x^n - x^{n+1}|^2)$.

Step 3. Update u^{n+1} and λ^{n+1} semi-implicitly.

$$(3.4) \quad \begin{aligned} \frac{\beta}{\sqrt{1 + (\partial_x h^{n*})^2}} \frac{h^{n+1} - h^{n*}}{\Delta t} &= \frac{\partial}{\partial x} \left(\frac{\partial_x h^{n+1}}{\sqrt{1 + (\partial_x h^{n*})^2}} \right) - \kappa(h^{n+1} \cos \theta_0 + x^{n+1} \sin \theta_0) + \lambda^{n+1}, \\ h^{n+1}(a^{n+1}) &= w(a^{n+1}), \quad h^{n+1}(b^{n+1}) = w(b^{n+1}), \\ \int_{a^{n+1}}^{b^{n+1}} u^{n+1}(x^{n+1}) dx^{n+1} &= \int_{a^0}^{b^0} u^0(x^0) dx^0, \end{aligned}$$

where the independent variable is $x^{n+1} \in (a^{n+1}, b^{n+1})$. For convenience, we provide a pseudo-code for this scheme in Appendix B.1.

Remark 3. From (3.1), we know for $n\Delta t < T$,

$$(3.5) \quad \begin{aligned} a^0 + \left(\sigma \sqrt{1 + \max_x |w_x|^2} - \max_x |w_x| \right) T &\leq a^n \leq a_0 + (1 + \sigma + \max_x |w_x|) T, \\ b^0 - (1 + \sigma + \max_x |w_x|) T &\leq b^n \leq b^0 - \left(\sigma \sqrt{1 + \max_x |w_x|^2} - \max_x |w_x| \right) T, \end{aligned}$$

so the explicit scheme for moving boundary is unconditionally stable.

Remark 4. We interpret the above time-discrete scheme as a De Giorgi's minimizing movement formulation for the gradient flow. For simplicity, consider the case $w(x) = 0, \theta_0 = 0$. Define the approximated energy functional at t^{n+1}

$$(3.6) \quad E_{n+1}(u) := \frac{1}{2} \int_{a^{n+1}}^{b^{n+1}} \frac{1 + u_x^2}{\sqrt{1 + (\partial_x u^{n*})^2}} dx + \frac{1}{2} \int_{a^{n+1}}^{b^{n+1}} \sqrt{1 + (\partial_x u^{n*})^2} dx + \sigma \int_{a^{n+1}}^{b^{n+1}} dx + \frac{\kappa}{2} \int_{a^{n+1}}^{b^{n+1}} u^2 dx,$$

and the distance function at t^{n+1}

$$(3.7) \quad \text{dist}_{n+1}(u, u^{n*}) := \beta \int_{a^{n+1}}^{b^{n+1}} \frac{(u - u^{n*})^2}{\sqrt{1 + (\partial_x u^{n*})^2}} dx.$$

Then for the updates in (3.4), u^{n+1} satisfies the minimizing movement problem (backward Euler scheme)

$$(3.8) \quad \min_{u \in H_0^1(a^{n+1}, b^{n+1})} \max_{\lambda} E_n(u) + \frac{1}{2\Delta t} \text{dist}_n(u, u^{n*}) - \lambda \left(\int_{a^{n+1}}^{b^{n+1}} u dx - V \right).$$

In other words, the update in (3.4) can be implemented by this minimizing problem.

3.1.2. Truncation analysis for first order scheme. In this section, we state the truncation error for the first order scheme, whose proof is in Appendix A.

Lemma 3.1. *Let $a(t^{n+1}), b(t^{n+1}), h(x^{n+1}, t^{n+1})$ for $x^{n+1} \in [a(t^{n+1}), b(t^{n+1})]$ be the exact solution to (2.39) evaluated at $t = t^{n+1}$ with initial data at $t = t^n$, $a^n, b^n, h^n(x^n)$ for $x^n \in [a^n, b^n]$. Then we have the first order truncation error estimates*

$$(3.9) \quad \begin{aligned} \frac{a(t^{n+1}) - a^n}{\Delta t} &= \sigma \sqrt{1 + (\partial_x w)_0^2} + \frac{1 + (\partial_x h^n)_0 (\partial_x w)_0}{\sqrt{1 + (\partial_x h^n)_0^2}} + O(\Delta t), \\ \frac{b(t^{n+1}) - b^n}{\Delta t} &= -\sigma \sqrt{1 + (\partial_x w)_N^2} - \frac{1 + (\partial_x h^n)_N (\partial_x w)_N}{\sqrt{1 + (\partial_x h^n)_N^2}} + O(\Delta t), \end{aligned}$$

$$(3.10) \quad \begin{aligned} &\frac{\beta}{\sqrt{1 + (\partial_x h^{n*})^2}} \frac{h(t^{n+1}) - h^{n*}}{\Delta t} \\ &= \frac{\partial}{\partial x} \left(\frac{\partial_x h(t^{n+1})}{\sqrt{1 + (\partial_x h^{n*})^2}} \right) - \kappa(h(t^{n+1})) \cos \theta_0 + x^{n+1} \sin \theta_0 + \lambda(t^{n+1}) + O(\Delta t), \\ &\quad x^{n+1} \in [a(t^{n+1}), b(t^{n+1})], \end{aligned}$$

where h^{n*} and x^n are given by

$$\begin{aligned} h^{n*}(x^{n+1}) &:= h^n(x^n) + \partial_x h^n(x^n)(x^{n+1} - x^n), \\ x^n &= a^n + \frac{b^n - a^n}{b(t^{n+1}) - a(t^{n+1})}(x^{n+1} - a(t^{n+1})) \in [a^n, b^n]. \end{aligned}$$

For simplicity, $h(t^{n+1})$ represents $h(\cdot, t^{n+1})$ in the lemma above and the remaining contents. By mapping moving domain to a fixed domain $Z = \frac{x-a(t)}{b(t)-a(t)} \in [0, 1]$ for any $x \in [a(t), b(t)]$, the proof of this lemma is standard so we put it in Appendix A.

3.2. Second order numeric algorithm based on a predictorcorrector method with an unconditionally stable explicit boundary moving. In this section, we use the predictorcorrector method to obtain a second order scheme. With the notations in Table 1, we still approximate $a(t^n), b(t^n)$ by a^n, b^n respectively and approximate $h(x^n, t^n)$ by $h^n(x^n)$ for $x^n \in (a^n, b^n)$. However, it is more convenient to use a fixed domain variable $Z = \frac{x-a(t)}{b(t)-a(t)} \in [0, 1]$ for any $x \in [a(t), b(t)]$. Denote $U(Z, t) := h(x, t)$. We will first present the derivation of the second order scheme based on the relation

$$(3.11) \quad Z = Z(x^{n+1}, t^{n+1}) = Z(x^n, t^n) = Z(x^{n+\frac{1}{2}}, t^{n+\frac{1}{2}}).$$

3.2.1. Derivation of a second order scheme based on the predictor-corrector method for DAEs with an inexact algebraic solver. To design a second order scheme, we illustrate the idea using the predictor-corrector method for an analogous DAEs. Assume we have an exact DAEs

$$(3.12) \quad \dot{b} = f(b, u), \quad 0 = g(b, u),$$

where the second algebraic equation is equivalent to $u = G(b)$ for some function G . However, in practice, one may not solve $u = G(b)$ exactly, which is to solve a mean curvature flow in our case. Therefore, we design the predictor-corrector method to solve a DAEs with an inexact algebraic

solver. Given b^n, u^n such that $u^n = G(b^n) + O(\Delta t^2)$.

Step 1. Solve the predictor \tilde{b}^{n+1} by forward Euler

$$(3.13) \quad \frac{\tilde{b}^{n+1} - b^n}{\Delta t} = f(b^n, u^n).$$

Step 2. Obtain the predictor \tilde{u}^{n+1} by solving algebraic equation up to a second order accuracy

$$(3.14) \quad \tilde{u}^{n+1} = G(\tilde{b}^{n+1}) + O(\Delta t^2).$$

Step 3. Solve the corrector b^{n+1} by the trapezoidal method

$$(3.15) \quad \frac{b^{n+1} - b^n}{\Delta t} = \frac{1}{2}[f(b^n, u^n) + f(\tilde{b}^{n+1}, \tilde{u}^{n+1})].$$

Step 4. Obtain the corrector u^{n+1} by solving the algebraic equation up to a second order accuracy

$$(3.16) \quad u^{n+1} = G(b^{n+1}) + O(\Delta t^2).$$

Indeed, we show the second order error estimate of this scheme below. Denote function $f(b, u) = f(b, G(b)) =: F(b)$. Then from (3.15), we have

$$(3.17) \quad \begin{aligned} \frac{b^{n+1} - b^n}{\Delta t} &= \frac{1}{2}[f(b^n, u^n) + f(\tilde{b}^{n+1}, \tilde{u}^{n+1})] \\ &= \frac{1}{2}[f(b^n, G(b^n)) + f(\tilde{b}^{n+1}, G(\tilde{b}^{n+1}))] + O(\Delta t^2) \\ &= \frac{1}{2}[F(b^n) + F(\tilde{b}^{n+1})] + O(\Delta t^2), \end{aligned}$$

which gives the second order accuracy for b^{n+1} and thus u^{n+1} .

3.2.2. Derivation of the second order accuracy for the semi-Lagrange term. Now we derive the second order scheme based on (3.11). First, consider the semi-Lagrange term

$$(3.18) \quad \partial_t h(x^{n+\frac{1}{2}}, t^{n+\frac{1}{2}}) = \partial_t U(Z, t^{n+\frac{1}{2}}) + \partial_Z U(Z, t^{n+\frac{1}{2}}) \partial_t Z(x^{n+\frac{1}{2}}, t^{n+\frac{1}{2}}) =: I_1 + I_2 I_3,$$

where $I_1 = \partial_t U(Z, t^{n+\frac{1}{2}})$ can be approximated by

$$I_1 = \frac{U(Z, t^{n+1}) - U(Z, t^n)}{\Delta t} + O(\Delta t^2) = \frac{h^{n+1}(x^{n+1}) - h^n(x^n)}{\Delta t} + O(\Delta t^2),$$

$I_2 = \partial_Z U(Z, t^{n+\frac{1}{2}})$ can be approximated by

$$\begin{aligned} I_2 &= \frac{1}{2} \partial_Z [U(Z, t^n) + U(Z, t^{n+1})] + O(\Delta t^2) \\ &= \frac{1}{2} [\partial_x h^n(x^n)(b^n - a^n) + \partial_x \tilde{h}^{n+1}(\tilde{x}^{n+1})(\tilde{b}^{n+1} - \tilde{a}^{n+1})] + O(\Delta t^2) \end{aligned}$$

since $|\tilde{x}^{n+1} - x^{n+1}| = O(\Delta t^2)$ due to (A.14). Notice $x^{n+\frac{1}{2}} - a^{n+\frac{1}{2}} = \frac{Z}{2}(b^{n+1} - a^{n+1})(b^n - a^n) \left(\frac{1}{b^{n+1} - a^{n+1}} + \frac{1}{b^n - a^n} \right)$ and the relation $a^{n+1} - a^{n+\frac{1}{2}} = a^{n+\frac{1}{2}} - a^n = \frac{a^{n+1} - a^n}{2}$. The last term

$I_3 = \partial_t Z(x^{n+\frac{1}{2}}, t^{n+\frac{1}{2}})$ in (3.18) can be approximated by

$$\begin{aligned}
I_3 &= \left(\frac{x^{n+\frac{1}{2}} - a^{n+1}}{b^{n+1} - a^{n+1}} - \frac{x^{n+\frac{1}{2}} - a^n}{b^n - a^n} \right) + O(\Delta t^2) \\
&= (x^{n+\frac{1}{2}} - a^{n+\frac{1}{2}}) \left(\frac{1}{b^{n+1} - a^{n+1}} - \frac{1}{b^n - a^n} \right) - \frac{a^{n+1} - a^n}{2} \left(\frac{1}{b^{n+1} - a^{n+1}} + \frac{1}{b^n - a^n} \right) + O(\Delta t^2) \\
&= -\frac{1}{2} \left(\frac{1}{b^{n+1} - a^{n+1}} + \frac{1}{b^n - a^n} \right) [(a^{n+1} - a^n) + Z((b^{n+1} - a^{n+1}) - (b^n - a^n))] + O(\Delta t^2) \\
&= -\frac{1}{2} \left(\frac{1}{b^{n+1} - a^{n+1}} + \frac{1}{b^n - a^n} \right) (x^{n+1} - x^n) + O(\Delta t^2).
\end{aligned}$$

Therefore, we can define the intermedia variable

$$\begin{aligned}
(3.19) \quad \tilde{h}^{n*}(x^{n+1}) &:= h^n(x^n) + \frac{1}{4} (x^{n+1} - x^n) \cdot \\
&\quad \left[\partial_x h^n(x^n) \left(1 + \frac{b^n - a^n}{\tilde{b}^{n+1} - \tilde{a}^{n+1}} \right) + \partial_x \tilde{h}^{n+1}(\tilde{x}^{n+1}) \left(1 + \frac{\tilde{b}^{n+1} - \tilde{a}^{n+1}}{b^n - a^n} \right) \right].
\end{aligned}$$

Indeed, one can further give the second order spatial discretization of $\tilde{h}^{n*}(x^{n+1})$ to see it has a similar form with (3.3). Notice the second order spatial discretizations for I_2, I_3 are

$$\begin{aligned}
I_2 &= \frac{N}{4} (h_{j+1}^n - h_{j-1}^n + \tilde{h}_{j+1}^{n+1} - \tilde{h}_{j-1}^{n+1}) + O(\Delta t^2 + \frac{1}{N^2}), \\
I_3 &= -\frac{1}{2} \left(\frac{1}{b^{n+1} - a^{n+1}} + \frac{1}{b^n - a^n} \right) [(a^{n+1} - a^n) + j(h^{n+1} - h^n)] + O(\Delta t^2).
\end{aligned}$$

Define the second order spatial discretization

$$(3.20) \quad \tilde{h}^{n*}(x_j^{n+1}) := h^n(x_j^n) + \frac{1}{8} \left(\frac{1}{\tau^{n+1}} + \frac{1}{\tau^n} \right) (h_{j+1}^n - h_{j-1}^n + \tilde{h}_{j+1}^{n+1} - \tilde{h}_{j-1}^{n+1}) [(a^{n+1} - a^n) + j(\tau^{n+1} - \tau^n)].$$

In summary, we have the second order approximation

$$(3.21) \quad \partial_t h(x^{n+\frac{1}{2}}, t^{n+\frac{1}{2}}) = \frac{h^{n+1}(x^{n+1}) - \tilde{h}^{n*}}{\Delta t} + O(\Delta t^2).$$

3.2.3. Second order predictor-corrector scheme and unconditional stability for explicit boundary moving. Now we present the second order scheme with continuous spatial variables.

Step 1. Predictor. Since we show the nonlinear elliptic solver in motion by mean curvature needs second order accuracy in Section 3.2.1, we repeat the first order scheme in Section 3.1 to update a^{n+1}, b^{n+1} using (3.1) but replace the semi-implicit elliptic solver by an implicit nonlinear elliptic solver, i.e.,

$$\begin{aligned}
(3.22) \quad \frac{\beta}{\sqrt{1 + (\partial_x h^{n+1})^2}} \frac{h^{n+1} - h^{n*}}{\Delta t} &= \frac{\partial}{\partial x} \left(\frac{\partial_x h^{n+1}}{\sqrt{1 + (\partial_x h^{n+1})^2}} \right) - \kappa(h^{n+1} \cos \theta_0 + x^{n+1} \sin \theta_0) + \lambda^{n+1}, \\
h^{n+1}(a^{n+1}) &= w(a^{n+1}), \quad h^{n+1}(b^{n+1}) = w(b^{n+1}), \\
\int_{a^{n+1}}^{b^{n+1}} u^{n+1}(x^{n+1}) dx^{n+1} &= \int_{a^0}^{b^0} u^0(x^0) dx^0,
\end{aligned}$$

where the independent variable is $x^{n+1} \in (a^{n+1}, b^{n+1})$. Denote the results as the predictor $\tilde{a}^{n+1}, \tilde{b}^{n+1}, \tilde{h}^{n+1}(\tilde{x}^{n+1})$ for $\tilde{x}^{n+1} \in [\tilde{a}^{n+1}, \tilde{b}^{n+1}]$. To solve (3.22), one can use the Newton iteration or solve (3.4) by replacing the stretching term $\frac{1}{\sqrt{1+(\partial_x h^{n*})^2}}$ iteratively after updating.

Step 2. Explicit boundary moving. Compute the one-side approximated derivative of h^n at b^n and a^n , denoted as $(\partial_x h^n)_N$ and $(\partial_x h^n)_0$. Then update

$$(3.23) \quad \begin{aligned} \frac{a^{n+1} - a^n}{\Delta t} &= \frac{1}{2} \left\{ \sigma \sqrt{1 + (\partial_x w)_0^2} + \sigma \sqrt{1 + (\partial_x \tilde{w})_0^2} + \frac{1 + (\partial_x h^n)_0 (\partial_x w)_0}{\sqrt{1 + (\partial_x h^n)_0^2}} + \frac{1 + (\partial_x \tilde{h}^{n+1})_0 (\partial_x \tilde{w})_0}{\sqrt{1 + (\partial_x \tilde{h}^{n+1})_0^2}} \right\}, \\ \frac{b^{n+1} - b^n}{\Delta t} &= -\frac{1}{2} \left\{ \sigma \sqrt{1 + (\partial_x w)_N^2} + \sigma \sqrt{1 + (\partial_x \tilde{w})_N^2} + \frac{1 + (\partial_x h^n)_N (\partial_x w)_N}{\sqrt{1 + (\partial_x h^n)_N^2}} + \frac{1 + (\partial_x \tilde{h}^{n+1})_N (\partial_x \tilde{w})_N}{\sqrt{1 + (\partial_x \tilde{h}^{n+1})_N^2}} \right\} \\ &\quad \text{with } (\partial_x w)_0 := \partial_x w(x_0^n), (\partial_x \tilde{w})_0 := \partial_x w(\tilde{x}_0^{n+1}), (\partial_x w)_N := \partial_x w(x_N^n), (\partial_x \tilde{w})_N := \partial_x w(\tilde{x}_N^{n+1}). \end{aligned}$$

Step 3. Solve $h^{n+1}(x)$ semi-implicitly. With $h_0^{n+1} = w(x_0^{n+1})$, $h_N^{n+1} = w(x_N^{n+1})$,

$$(3.24) \quad \begin{aligned} &\beta \frac{h^{n+1} - h^{n*}}{\Delta t} \frac{1}{2} \left[\frac{1}{\sqrt{1 + (\partial_x h_j^n)^2}} + \frac{1}{\sqrt{1 + (\partial_x \tilde{h}_j^{n+1})^2}} \right] \\ &= \frac{1}{2} \frac{\partial}{\partial x} \left(\frac{\partial_x h^{n+1}}{\sqrt{1 + (\partial_x \tilde{h}^{n+1})^2}} + \frac{\partial_x h^n}{\sqrt{1 + (\partial_x h^n)^2}} \right) - \frac{\kappa}{2} [(h^{n+1} + h^n) \cos \theta_0 + (x^n + x^{n+1}) \sin \theta_0] + \lambda^{n+\frac{1}{2}}, \\ &\quad \int_{a^{n+1}}^{b^{n+1}} u^{n+1}(x^{n+1}) dx^{n+1} = \int_{a^0}^{b^0} u^0(x^0) dx^0, \end{aligned}$$

where h^{n*} is defined in (3.19) and the equality holds in the sense of changing variables to the fixed domain $Z = \frac{x-a(t)}{b(t)-a(t)} \in [0, 1]$ and $Z = Z(x^{n+1}, t^{n+1}) = Z(x^n, t^n) = Z(x^{n+\frac{1}{2}}, t^{n+\frac{1}{2}})$. For convenience, we provide a pseudo-code for this scheme in Appendix B.2.

Remark 5. From (3.23), we know for $n\Delta t < T$, we have exact the same bound for the stability estimate in (3.5), so the explicit scheme for moving boundary in the second order scheme is still unconditionally stable.

3.2.4. Second order truncation error estimates for the predictor-corrector method. The strategy of the second order truncation error estimates is same as that of Lemma 3.1 by noticing in a fixed domain in terms of $Z \in [0, 1]$ the predictor-corrector method gives us a second order scheme and then we prove the mapping from Z to x^{n+1} keep the second order accuracy. For completeness, we put the proof of Lemma 3.2 in Appendix A.

Lemma 3.2. *Let $a(t^{n+1}), b(t^{n+1}), h(x^{n+1}, t^{n+1}) = U(Z, t^{n+1})$ for $x^{n+1} \in [a(t^{n+1}), b(t^{n+1})]$ be the exact solution to (2.39) evaluated at $t = t^{n+1}$ with initial data at $t = t^n$, $a^n, b^n, h^n(x^n)$ for $x^n \in [a^n, b^n]$. Let $\tilde{a}^{n+1}, \tilde{b}^{n+1}$ be the predictor obtained by (3.1) and $\tilde{h}^{n+1}(\tilde{x}^{n+1}) = \tilde{U}^{n+1}(Z)$ for $\tilde{x}^{n+1} \in [\tilde{a}^{n+1}, \tilde{b}^{n+1}]$ be the predictor obtained by (3.22). Then we have the second order truncation error*

estimates

$$\begin{aligned}
(3.25) \quad \frac{a(t^{n+1}) - a^n}{\Delta t} &= \frac{1}{2} \left\{ \sigma \sqrt{1 + (\partial_x w)_0^2} + \sigma \sqrt{1 + (\partial_x \tilde{w})_0^2} \right. \\
&\quad \left. + \frac{1 + (\partial_x h^n)_0 (\partial_x w)_0}{\sqrt{1 + (\partial_x h^n)_0^2}} + \frac{1 + (\partial_x \tilde{h}^{n+1})_0 (\partial_x \tilde{w})_0}{\sqrt{1 + (\partial_x \tilde{h}^{n+1})_0^2}} \right\} + O(\Delta t^2), \\
\frac{b(t^{n+1}) - b^n}{\Delta t} &= -\frac{1}{2} \left\{ \sigma \sqrt{1 + (\partial_x w)_N^2} + \sigma \sqrt{1 + (\partial_x \tilde{w})_N^2} \right. \\
&\quad \left. + \frac{1 + (\partial_x h^n)_N (\partial_x w)_N}{\sqrt{1 + (\partial_x h^n)_N^2}} + \frac{1 + (\partial_x \tilde{h}^{n+1})_N (\partial_x \tilde{w})_N}{\sqrt{1 + (\partial_x \tilde{h}^{n+1})_N^2}} \right\} + O(\Delta t^2),
\end{aligned}$$

where $(\partial_x w)_0 := \partial_x w(x_0^n)$, $(\partial_x \tilde{w})_0 := \partial_x w(\tilde{x}_0^{n+1})$, $(\partial_x w)_N := \partial_x w(x_N^n)$, $(\partial_x \tilde{w})_N := \partial_x w(\tilde{x}_N^{n+1})$ and

$$\begin{aligned}
(3.26) \quad \beta \frac{h(t^{n+1}) - h^{n*}}{\Delta t} &= \frac{1}{2} \left[\frac{1}{\sqrt{1 + (\partial_x h^n)^2}} + \frac{1}{\sqrt{1 + (\partial_x \tilde{h}^{n+1})^2}} \right] = \frac{1}{2} \frac{\partial}{\partial x} \left(\frac{\partial_x h^{n+1}}{\sqrt{1 + (\partial_x \tilde{h}^{n+1})^2}} + \frac{\partial_x h^n}{\sqrt{1 + (\partial_x h^n)^2}} \right) \\
&\quad - \frac{\kappa}{2} [(h^{n+1} + h^n) \cos \theta_0 + (x^n + x^{n+1}) \sin \theta_0] + \lambda^{n+1} + O(\Delta t^2),
\end{aligned}$$

where h^{n*} is defined in (3.19).

4. VALIDATIONS AND COMPUTATIONS

In this section, we will first use the DAEs solution for the quasi-static dynamics to check the second order accuracy of the numerical schemes proposed in the last section. Then we design several challenging and important examples: (i) a periodic breathing droplet with a closed formula solution and a long-time computational validation; (ii) dynamics of a droplet on an inclined rough surface and in a Utah teapot; (iii) Kelvin pendant droplet with repeated bulges and the corresponding desingularized DAEs solver for quasi-static dynamics based on horizontal graph representation.

4.1. Desingularized DAEs formula and accuracy check for the quasi-static dynamics.

In this section, we will first derive the DAEs for the quasi-static dynamics using a desingularized formula. Then we give an accuracy check for the case $w(x) = 0$ and $\theta_0 = 0$ using the corresponding quasi-static solutions, which can be obtained using the desingularized DAEs solver.

4.1.1. *DAEs description of the quasi-static dynamics.* Given volume V , assume $w(x) = 0$ and $\theta_0 = 0$. If we assume quasi-static condition $\beta = 0$ in (2.39), the quasi-static droplet profile u for any fixed t satisfies

$$\begin{aligned}
(4.1) \quad \frac{d}{dx} \left(\frac{\partial_x u}{\sqrt{1 + (\partial_x u)^2}} \right) - \kappa u + \lambda(t) &= 0, \quad a(t) < x < b(t), \\
\int_{a(t)}^{b(t)} u(x, t) dx &= V,
\end{aligned}$$

with boundary condition $u(a(t), t) = u(b(t), t) = 0$. Multiplying (4.1) by u and integration by parts give immediately that $\kappa > 0$ implies $\lambda > 0$. In this subsection, we will derive the following DAEs

for $b(t), \lambda(t), u_m(t)$ in three steps, which completely describes the quasi-static motion

$$(4.2) \quad \begin{aligned} b'(t) &= -\sigma - \cos \theta(t) = -\sigma - \frac{\kappa u_m^2(t)}{2} + \lambda(t)u_m(t) - 1, \\ u_m b - \frac{V}{2} &= \sqrt{2} \int_0^{u_m} \sqrt{\frac{u_m - u}{2\lambda - \kappa(u_m + u)}} \frac{J(u)}{\sqrt{1 + J(u)}} du, \\ b &= \sqrt{2} \int_0^{u_m} \frac{1}{\sqrt{u_m - u}} \frac{1}{\sqrt{2\lambda - \kappa(u_m + u)}} \frac{J(u)}{\sqrt{1 + J(u)}} du, \end{aligned}$$

where $u_m(t)$ is the maximal point of $u(x, t)$.

Step 1. Symmetry of the quasi-static profile for fixed $t > 0$. It is easy to see (4.1) is translation invariant for $x \rightarrow x + \epsilon$, so initially we assume $a(0) = -b(0) < 0$ without loss of generality. Due to the reflection invariant under $x \rightarrow -x$, the solution $u(x)$ is even. Hence $\partial_x u(-x) = -\partial_x u(x)$ and $a'(t) = -b'(t)$. Therefore we always have $a(t) = -b(t) < 0$.

Step 2. The maximal height for equilibrium. Combining the symmetry in Step 1 and the gradient flow for the quasi-static dynamics (2.28), we have

$$(4.3) \quad b'(t) = -\frac{\partial \mathcal{F}_r}{\partial b} = -(G - \partial_x u \partial_{u_x} G)|_{b(t)} = -\sigma - \frac{1}{\sqrt{1 + (\partial_x u)^2}} \Big|_{b(t)},$$

where $u(x, t)$ satisfies (4.1) with the boundary condition $u(-b(t), t) = u(b(t), t) = 0$.

Multiplying $\partial_x u$ in (4.1) and integration by parts show that

$$(4.4) \quad \frac{\kappa u^2}{2} + \frac{1}{\sqrt{1 + (\partial_x u)^2}} - \lambda(t)u = C(t).$$

For θ defined as $\tan \theta = -\partial_x u|_{x=b}$, this leads to

$$(4.5) \quad \cos \theta(t) = C(t) = \frac{\kappa u_m^2(t)}{2} - \lambda(t)u_m(t) + 1,$$

where $u_m(t)$ is the maximal point of $u(x, t)$. Combined with (4.3), we know

$$(4.6) \quad b'(t) = -\sigma - \cos \theta = -\sigma - C(t) = -\sigma - \frac{\kappa u_m^2(t)}{2} + \lambda(t)u_m(t) - 1.$$

If $\lambda(t) \rightarrow \lambda^*$ and $b'(t) \rightarrow 0$ then $u_m = u_e := \frac{\lambda^*}{\kappa} + \sqrt{-\frac{2}{\kappa}(1 + \sigma) + (\frac{\lambda^*}{2})^2}$.

Step 3. Hodograph transformation and desingularization. Now we use the hodograph transformation to give a closed formula for the quasi-static profile with a given u_m .

Consider the inverse function of $u(x, t)$ for $0 \leq x \leq b(t)$. From $\frac{du}{dx} = \frac{dX}{du}$ and (4.4),

$$(4.7) \quad \left(\frac{dX}{du} \right)^2 = \frac{(\cos \theta(t) - \frac{\kappa u^2}{2} + \lambda(t)u)^2}{1 - (\cos \theta(t) - \frac{\kappa u^2}{2} + \lambda(t)u)^2} = \frac{J(u)^2}{1 - J(u)^2},$$

where

$$(4.8) \quad J(u) := -\frac{\kappa}{2}(u^2 - u_m^2) + \lambda(t)(u - u_m) + 1 = -\frac{\kappa}{2}u^2 + \lambda(t)u + \cos \theta(t).$$

Assume we are always in the single graph representation setting, i.e. $\cos \theta(t) = C(t) = J(0) > 0$, which is $u_m(t) < \frac{\lambda(t) - \sqrt{\lambda(t)^2 - 2\kappa}}{\kappa}$ or $\lambda(t)^2 < 2\kappa$. Notice

$$(4.9) \quad 1 \geq J(u) \geq J(0) = 1 + \frac{\kappa u_m^2}{2} - \lambda(t)u_m > 0.$$

Since $\partial_x u \leq 0$ for $0 \leq x \leq b(t)$,

$$(4.10) \quad \frac{dX}{du} = \frac{-J(u)}{\sqrt{1-J(u)^2}}.$$

Recall the dynamic equation for the endpoint (4.6). To solve b, u_m and λ together, we need another equation based on the volume preserving condition in (4.1). On one hand, by the volume constraint we know,

$$(4.11) \quad \frac{V}{2} = \int_0^{u_m} \frac{du}{du} X(u) du = - \int_0^{u_m} u X_u du.$$

To desingularize $X_u(u_m) = \infty$, we use the following formula

$$(4.12) \quad \begin{aligned} u_m b - \frac{V}{2} &= u_m X(0) - \frac{V}{2} = \int_0^{u_m} (u - u_m) X_u du \\ &= \int_0^{u_m} (u - u_m) \frac{-J(u)}{\sqrt{1-J(u)^2}} du \\ &= \sqrt{2} \int_0^{u_m} \sqrt{\frac{u_m - u}{2\lambda - \kappa(u_m + u)}} \frac{J(u)}{\sqrt{1+J(u)}} du. \end{aligned}$$

On the other hand, to desingularize $\frac{dx}{du}$ in the numerical implementation, denote $w := \sqrt{u_m - u}$. Then we have

$$(4.13) \quad J(u) = 1 - [\lambda - (2u_m - w^2) \frac{\kappa}{2}] w^2.$$

It is easy to check

$$\frac{dw}{dx} = \frac{1}{2w} \frac{\sqrt{1-J(u)^2}}{J} = \frac{1}{2w} \frac{\sqrt{1-J(u)}\sqrt{1+J(u)}}{J} = \frac{\sqrt{2\lambda - \kappa(2u_m - w^2)}}{2\sqrt{2}} \frac{\sqrt{1+J(u)}}{J(u)} > 0$$

for all $0 \leq x \leq b$. Thus there is no singularity for $\frac{dx}{dw}$. Integrating x from 0 to b while w from 0 to $\sqrt{u_m}$, we have

$$(4.14) \quad b = \int_0^{\sqrt{u_m}} \frac{2\sqrt{2}}{\sqrt{2\lambda - \kappa(u_m + u)}} \frac{J(u)}{\sqrt{1+J(u)}} dw,$$

which is equivalent to

$$(4.15) \quad b = \sqrt{2} \int_0^{u_m} \frac{1}{\sqrt{u_m - u}} \frac{1}{\sqrt{2\lambda - \kappa(u_m + u)}} \frac{J(u)}{\sqrt{1+J(u)}} du.$$

However, to implement this singular integral, we use the desingularized midpoint rule suggested by $w = \sqrt{u_m - u}$. Let $\tau = \frac{\sqrt{u_m}}{N}$, $w_{i+\frac{1}{2}} := (i + \frac{1}{2})\tau$ and $u_{i+\frac{1}{2}} := u_m - w_{i+\frac{1}{2}}^2$. Then (4.14) can be approximated by

$$(4.16) \quad b \approx 2\sqrt{2} \sum_{i=0}^{N-1} \frac{\tau}{\sqrt{2\lambda - \kappa(u_m + u_{i+\frac{1}{2}})}} \frac{J(u_{i+\frac{1}{2}})}{\sqrt{1+J(u_{i+\frac{1}{2}})}}.$$

Combining ODE (4.6) and two algebraic equations (4.12) and (4.14), we obtain DAEs (4.2) for $b(t), \lambda(t), u_m(t)$. With the desingularized formula (4.16), there is no singularity in the DAEs, so it can be solved efficiently and accurately by any ODE solver such as *ode15s* in Matlab, whose results

will be used to check the accuracy for our PDE solvers. Furthermore, by (4.10) and $X(u_m) = 0$, we can solve the capillary surface $X(u, t)$ by the integral formula

$$(4.17) \quad X(u, \cdot) = \int_u^{u_m} \frac{J(y)}{\sqrt{1 - J(y)^2}} dy.$$

Finally, we give the equilibrium solution for DAEs (4.2). Taking $b'(t) = 0$ in (4.6), we have the algebraic equation

$$(4.18) \quad -\frac{\kappa u_m^2(t)}{2} + \lambda(t)u_m(t) = \sigma + 1.$$

This, together with (4.14) and (4.12), we can determine uniquely the steady solution (b, u_m, λ) .

4.1.2. *Accuracy check between DAEs and 1st/2nd order PDE solvers.* We first use the DAEs solver *ode15s* in Matlab to solve the solution to DAEs (4.2) with the initial data

$$(4.19) \quad \theta_{in} = \frac{1.3\pi}{8}, \quad u_m(0) = 1$$

and the final Young's angle $\theta_f = \frac{3.9\pi}{8}$. The parameters in DAEs (4.2) are

$$(4.20) \quad \kappa = 0, \quad \sigma = -\cos(\theta_f).$$

With $u_m(0) = 1$, we start the DAEs by first solving the initial data $b(0)$ and $\lambda(0)$ from (4.2). The final time in *ode15s* is $T = 1$. We obtain $b(0) = 3.832203449327490$, $b(1) = 3.065160982538375$.

Compared with the DAEs solution, we show below the accuracy check for the first order scheme in Section 3.1.1 and the second order scheme in Section 3.2 in Table 2 and Table 3 respectively. We use the same parameters $\beta = 0$, $\kappa = 0$, initial angle $\theta_{in} = \frac{1.3\pi}{8}$, final Young's angle $\theta_Y = \frac{3.9\pi}{8}$, final time $T = 1$, and the same initial boundary $b(0) = 3.832203449327490$ in the first/second order scheme. For several M_n listed in the tables, we take time step as $\Delta t = \frac{T}{M_n}$ and moving grid size $\Delta x = \frac{b(t)-a(t)}{N_n}$ with $N_n = 8M_n$. The absolute error e_n between numeric solutions and the DAEs solution $b(1) = 3.065160982538375$ is listed in the second column of the tables. The corresponding order of accuracy $\alpha = \frac{\ln(e_n/e_{n+1})}{\ln(M_{n+1}/M_n)}$ is listed in the last column of the tables.

TABLE 2. Accuracy check: 1st order scheme in Section 3.1.1 v.s. exact quasi-static solution to (4.2) using *ode15s*. Parameters: $T = 1$, $\kappa = 0$, $\theta_Y = \frac{3.9\pi}{8}$, $\theta(0) = \frac{1.3\pi}{8}$, $b(0) = 3.832203449327490$, time step $\Delta t = \frac{T}{M}$, M listed on the table, moving grid size $\Delta x = \frac{b(t)-a(t)}{N}$, $N = 8M$. Absolute errors e_n are computed by comparing with $b(1) = 3.065160982538375$.

M	Error at $T = M\Delta t = 1$	Order of accuracy
40	$e_1 = 2.244 \times 10^{-3}$	
80	$e_2 = 1.129 \times 10^{-3}$	0.9918
160	$e_3 = 5.659 \times 10^{-4}$	0.9958
320	$e_4 = 2.834 \times 10^{-4}$	0.9979

TABLE 3. Accuracy check: 2nd order scheme in Section 3.2.3 v.s. exact quasi-static solution to (4.2) using *ode15s*. Parameters: $T = 1$, $\kappa = 0$, $\theta_Y = \frac{3.9\pi}{8}$, $\theta_{in} = \frac{1.3\pi}{8}$, $b(0) = 3.832203449327490$, time step $\Delta t = \frac{T}{M}$, M listed on the table, moving grid size $\Delta x = \frac{b(t)-a(t)}{N}$, $N = 8M$. Absolute errors e_n are computed by comparing with $b(1) = 3.065160982538375$.

M	Error at $T = M\Delta t = 1$	Order of accuracy
40	$e_1 = 3.416 \times 10^{-7}$	
80	$e_2 = 1.147 \times 10^{-7}$	1.5748
160	$e_3 = 3.241 \times 10^{-8}$	1.8234
320	$e_4 = 8.595 \times 10^{-9}$	1.9147

4.2. Breathing droplet: closed formula and long-time validation. In this section, we construct a breathing droplet solution motivated by the closed spherical cap formula and use this example to demonstrate the long time validation of our numerical schemes in Section 3.

Denote the mean curvature of the capillary surface u in the direction of outer normal as H , which is given by $H = -\nabla \cdot \left(\frac{\nabla u}{\sqrt{1+|\nabla u|^2}} \right)$ in the graph representation. Here u is the piecewise graph representation of capillary surface. When $\kappa = 0$, the governing equation for the quasi-static dynamics becomes $H = \lambda$, where λ is a function of t . This means the quasi-static profile has constant mean curvature $\lambda(t)$ everywhere on the capillary surface. Assume the initial droplet has the contact domain $\{x \in \mathbb{R}^{d-1}; |x| \leq b(0)\}$. Due to the rotation invariant for both equation and initial contact domain, the solution will remain axially symmetric, denoted as $u(r, t)$. As a consequence, the quasi-static profile is a spherical cap, whose center may be above the ground. To describe this spherical cap solution, we denote the height of the center as $u^*(t) \in \mathbb{R}$. Furthermore, notice the mean curvature of a d -dimensional ball is $H = \frac{d-1}{R}$, where R is the radius of the spherical cap.

Consider the partially wetting case in 3D when the droplet is represented by the single graph function $u(r, t)$, $0 \leq r \leq b(t)$. Using $H = -\nabla \cdot \left(\frac{\nabla u}{\sqrt{1+|\nabla u|^2}} \right) = -\frac{1}{r} \partial_r \left(\frac{r \partial_r u}{\sqrt{1+(\partial_r u)^2}} \right) = \lambda(t) = \frac{2}{R(t)}$, we can solve

$$(4.21) \quad u_m(t) - u(r, t) = \frac{2}{\lambda(t)} \left(1 - \sqrt{1 - \left(\frac{\lambda(t)r}{2} \right)^2} \right).$$

Then $u^*(t) = \frac{2}{\lambda(t)} - u_m(t)$ and we have

$$(4.22) \quad (u(r, t) - u^*(t))^2 + r^2 = R(t)^2.$$

For the droplet in the non-wetting case, the capillary surface can not be expressed uniquely by the graph function $u(r)$. In the non-wetting case, in which the center $u^*(t)$ is above the ground, one shall use two graph representation (with same notations) for $0 \leq u \leq u^*(t)$ and $u^*(t) \leq u \leq u_m$ respectively; see also the horizontal graph representation in Section 4.5. The spherical cap formula (4.22) holds true for these two pieces.

To efficiently formulate the DAEs for the quasi-static profile, denote contact angle θ as $\tan \theta = -\partial_r u|_{r=b}$. Then by elementary calculation we obtain the classical spherical cap volume formula in

3D

$$(4.23) \quad \frac{V}{b^3} = \frac{\pi}{3 \sin^3 \theta} (2 - 3 \cos \theta + \cos^3 \theta).$$

With this θ , the boundary motion (4.3) becomes

$$(4.24) \quad b'(t) = -\sigma - \frac{1}{\sqrt{1 + (\tan \theta)^2}} = \cos \theta_Y - \cos \theta.$$

In 2D case, the volume formula becomes

$$(4.25) \quad \frac{V}{X(0)^2} = \frac{\theta}{\sin^2 \theta} - \frac{\cos \theta}{\sin \theta}.$$

4.2.1. *Construct an exact breathing droplet solution and compare with numerical simulations.* Motivated by the spherical cap solution in the last subsection, with a prescribed contact angle $\theta(t)$, we construct a breathing spherical cap solution satisfying

$$(4.26) \quad \begin{aligned} \beta \frac{\partial_t u(x, t)}{\sqrt{1 + (\partial_x u)^2}} &= \frac{\partial}{\partial x} \left(\frac{\partial_x u}{\sqrt{1 + (\partial_x u)^2}} \right) - \kappa(t)u + \lambda(t), \quad x \in (-b(t), b(t)), \\ b'(t) &= -\sigma(t) - \frac{1}{\sqrt{1 + (\partial_x u)^2}}, \quad x = b(t), \\ &\int_{-b(t)}^{b(t)} u(x, t) dx = V, \end{aligned}$$

where the parameters $\kappa(t), \sigma(t)$ will be determined below. Here we consider only the partially wetting case $0 < \theta(t) \leq \frac{\pi}{2}$.

Now we proceed to derive the formula $\kappa(t), \sigma(t)$ for this breathing droplet. Given $\theta(t)$ with oscillations, we will first calculate $u(x, t)$ and $b(t)$ from the spherical cap formula and then find $\kappa(t)$ and $\sigma(t)$ such that the PDE (4.26) holds with the Lagrangian multiplier $\lambda(t)$.

Step 1. Given the initial data $\theta(0)$ and $b(0)$. Calculate volume V from (4.25).

Step 2. Calculate $u(x, t)$ and $b(t)$. From the spherical cap formula (4.25)

$$(4.27) \quad b(t) = \sqrt{V \frac{1 - \cos(2\theta(t))}{2\theta(t) - \sin(2\theta(t))}},$$

and from $R(t) = \frac{b(t)}{\sin \theta(t)}$, $R(t) - u_m(t) = R \cos \theta(t)$ we have

$$(4.28) \quad u(x, t) = -R(t) \cos \theta(t) + \sqrt{R(t)^2 - x^2}, \quad x \in (-b(t), b(t)).$$

This construction automatically preserves the volume V and we know

$$(4.29) \quad u_x = \frac{-x}{\sqrt{R(t)^2 - x^2}}, \quad \sqrt{1 + (u_x)^2} = \frac{R(t)}{\sqrt{R(t)^2 - x^2}}, \quad \frac{u_x}{\sqrt{1 + u_x^2}} = \frac{-x}{R(t)}.$$

TABLE 4. Ten points used in Bézier curve fitting of geometry of the Utah teapot

i	1	2	3	4	5	6	7	8	9	10
x_i	-2	$-\frac{4}{3}$	$-\frac{2}{3}$	0	$\frac{2}{3}$	$\frac{4}{3}$	2	2.655	2.846	4
y_i	0.78	0	0	0	0	0	0.78	1.142	2.146	2.5

Step 3. We find $\kappa(t), \sigma(t)$ and $\lambda(t)$ such that (4.26) holds. From the formula in Step 2, we can solve

$$\begin{aligned}
 \kappa(t) &= -\beta \left(\frac{b(t)^2}{V} \cos \theta(t) \dot{\theta}(t) + \sin \theta(t) \right), \\
 \lambda(t) &= \beta \left(-\frac{b(t)^2}{V} \sin \theta(t) \dot{\theta}(t) + \cos \theta(t) \right) + \frac{\sin \theta(t)}{b(t)}, \\
 \sigma(t) &= -b(t) \dot{\theta}(t) \left(\cot \theta(t) - \frac{b(t)^2}{V} \right) - \cos \theta(t).
 \end{aligned}
 \tag{4.30}$$

Particularly, for the quasi-static case $\beta = 0$, we have

$$\kappa(t) = 0, \quad \lambda(t) = \frac{\sin \theta(t)}{b(t)}.
 \tag{4.31}$$

The constructed breathing droplet solution can be easily extended to 3D; see Appendix D.

Let the oscillated contact angle be $\theta(t) = \theta_{in} + A \sin t$, with $\theta_{in} = \frac{1.3\pi}{8}$, $A = 0.2$. Now we show the evolution of breathing droplet and the periodic recurrence for $[0, 30\pi]$. The dynamics of the breathing droplet in Fig. 2 is computed by the first order scheme in Section 3.1.1 with $\kappa(t), \sigma(t)$ in (4.30) and with initial contact domain $[-3, 3]$ and initial profile calculated by (4.28) for $t = 0$. The parameters in the PDE solver are $\beta = 0.1$, final time $T = 30\pi$, time step $\Delta t = \frac{T}{1500} = 0.0628$, $N = 1000$ for moving grids in $(a(t), b(t))$.

4.3. Capillary motion of a droplet in the Utah teapot. The Utah teapot is an important object in computer graphics history, whose 2D cross section can be completely described by several cubic Bézier curves. In this section, we will use the bottom and the mouth of the Utah teapot as the inclined rough substrate to demonstrate the competition between the gravitational effect and capillary effect for droplet with small Bond number.

We use four points (x_i, y_i) , $i = 1, \dots, 4$ to construct a cubic Bézier curve $(x(\ell), y(\ell))$ with parameter $\ell \in [0, 1]$. Denote the Bernstein basis polynomials as

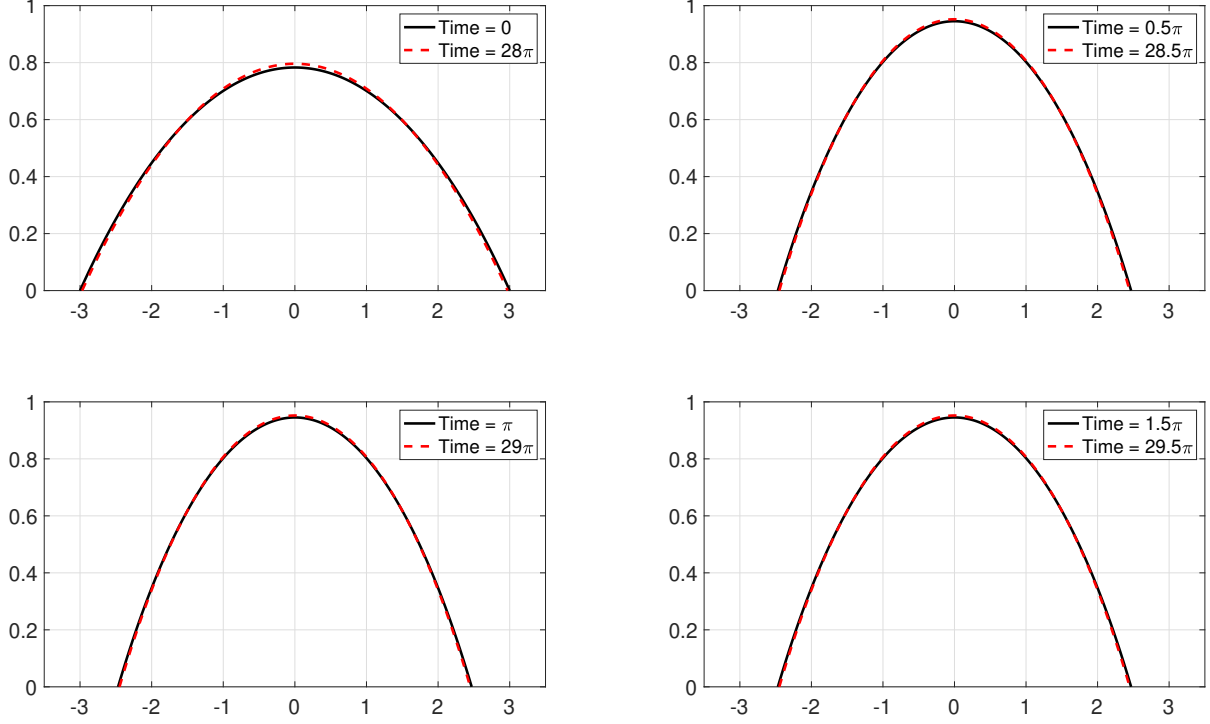
$$B_1(\ell) = (1 - \ell)^3, \quad B_2(\ell) = 3(1 - \ell)^2\ell, \quad B_3(\ell) = 3(1 - \ell)\ell^2, \quad B_4(\ell) = \ell^3.
 \tag{4.32}$$

Then the cubic Bézier curve is uniquely given by

$$x(\ell) = \sum_{i=1}^4 B_i(\ell)x_i, \quad y(\ell) = \sum_{i=1}^4 B_i(\ell)y_i.
 \tag{4.33}$$

Now we construct the bottom and the mouth of the Utah teapot using 10 points x_i, y_i , $i = 1, \dots, 10$ listed in Table 4. For the bottom of the teapot, we use (x_i, y_i) for $i = 1, \dots, 4$ and (x_i, y_i) for $i = 4, \dots, 7$. For the mouth of the teapot, we use (x_i, y_i) for $i = 7, \dots, 10$. Notice the inclined rough substrate is now expressed by parametric curve (4.33). Let $\ell(x)$ be the inverse function of $x(\ell)$, then $w(x) = y(\ell(x))$ in the first order and second order schemes. To evaluate function w at endpoint

FIGURE 2. Evolution of the breathing droplet and its periodic recurrence for $[0, 30\pi]$. Computed by the first order scheme in Section 3.1.1 with $\kappa(t)$ and $\sigma(t)$ in (4.30) and oscillated contact angle $\theta(t) = \theta_{in} + A \sin t$, with $\theta_{in} = \frac{1.3\pi}{8}$, $A = 0.2$. The parameters in the PDE solver are $\beta = 0.1$, $T = 30\pi$, $\Delta t = 0.0628$, $N = 1000$ for moving grids, initial domain $[-3, 3]$ and initial $u(x, 0)$ calculated by (4.28). Each subfigure shows the breathing droplet at time snapshots $[0, \frac{\pi}{2}, \pi, \frac{3\pi}{2}]$ and the recurrence after 15 periods.



a in the numerical implementation, one can use linear interpolation $a = (1 - \alpha)x(\ell_i) + \alpha x(\ell_{i+1})$ for some $\alpha \in [0, 1]$.

Now we take the physical parameters as $\kappa = 5$, $\beta = 0.2$ and the initial droplet as

$$(4.34) \quad h(x, 0) = 5.2(x - a(0))(b(0) - x) + w(a(0)) + \frac{[w(b(0)) - w(a(0))](x - a(0))}{b(0) - a(0)}$$

with initial endpoints $a(0) = 2.4, b(0) = 2.9$. The corresponding effective Bond number can be calculated by (2.36) with effective inclined angle $\theta_0 = 0.226\pi$, $\text{Bo} = 0.1312$. In the second order scheme, we use $N = 1000$ moving grids uniformly in $(a(t), b(t))$. We take final time as $T = 96$ with time step $\Delta t = 0.08$. Different capillary motions with different relative adhesion coefficients (upper) $\sigma = -0.8$ and (lower) $\sigma = -0.6$ are shown in Fig. 3 respectively. In each figure, the green line is the initial droplet, red lines are the evolution of the droplet at equal time intervals, and the blue line is the final droplet at $T = 96$.

4.4. Dynamics of droplets on an inclined rough surface. In this section, we show the contact angle hysteresis (CAH) for a droplet on inclined rough surfaces. Gravity will pull the droplet down while CAH will resist its motion. Therefore, one will observe the top of the droplet becomes thin

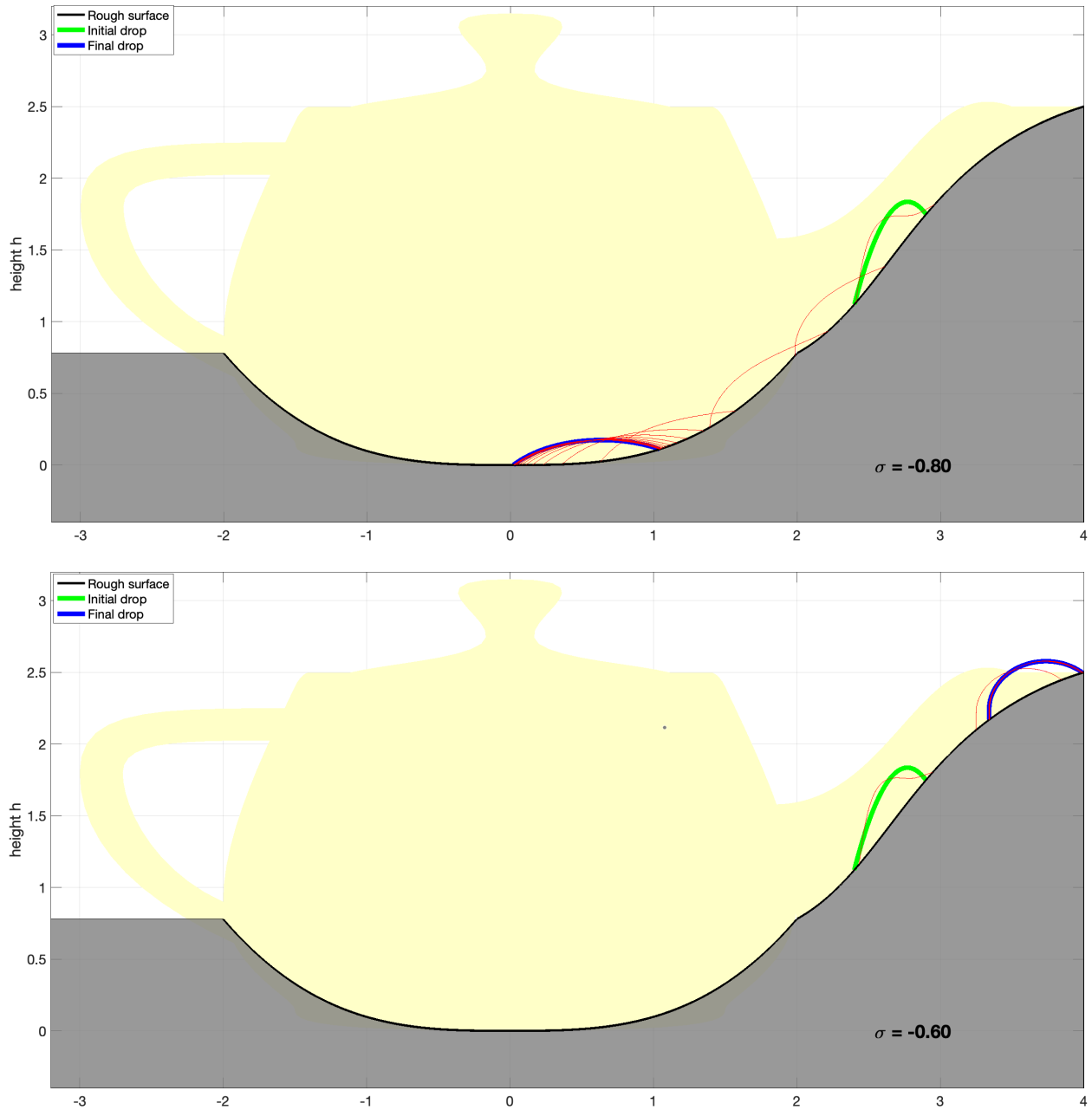


FIGURE 3. Evolution of a partially wetting droplet in the Utah teapot at equal time intervals using the second order time-space scheme in Section 3.2.3. Parameters: number of moving grids in drop $N = 1000$, time step $\Delta t = 0.08$, $\kappa = 5$, $\beta = 0.2$, bond number $Bo = 0.1312$, initial drop profile given in (4.34) with $a(0) = 2.4$, $b(0) = 2.9$, and final time $T = 96$. (upper) Gravity wins: relative adhesion coefficient $\sigma = -0.8$; (lower) capillary rise: relative adhesion coefficient $\sigma = -0.6$.

while the bottom of it becomes thick. Besides, the contact line speeds depend on both the contact angle θ_a, θ_b and the local slope of the rough surface θ_{0a}, θ_{0b} (in (2.39)), which changes constantly due to the boundary motion. Consequently, one can observe the contact line speed will change accordingly.

To demonstrate those phenomena, we take two typical rough surfaces

$$(4.35) \quad w_1(x) = A(\sin(kx) + \cos(2kx))^2, \quad A = 0.08, \quad k = 5,$$

$$(4.36) \quad w_2(x) = A(\sin(kx) + \sin(kx/2) + \cos(2kx)), \quad A = 0.1, \quad k = 5.$$

We take the physical parameters as $\kappa = 0.3$, $\beta = 0.3$ and initial droplet as

$$(4.37) \quad h(x, 0) = 0.08(x - a(0))(b(0) - x)(x^2 + 3x/2 + 1) + w(a(0)) + \frac{[w(b(0)) - w(a(0))](x - a(0))}{b(0) - a(0)}$$

with initial endpoints $a(0) = -3$, $b(0) = 3$. The corresponding effective Bond number can be calculated by (2.36) with effective inclined angle $\theta_0 = 0.3$. The evolution of partially wetting droplets are computed by the second order scheme in Section 3.2.3. We take final time as $T = 96$ with time step $\Delta t = 0.08$ and use $N = 1000$ moving grids uniformly in $(a(t), b(t))$. With relative adhesion coefficient $\sigma = -0.95$, we show in Fig. 4 droplets on (upper) rough surface $w_1(x)$ in (4.35) and (lower) rough surface $w_2(x)$ in (4.36) respectively. In each figure, green line is the initial droplet, red lines are the evolution of the droplet at equal time intervals, and the blue line is the final droplet at $T = 96$.

4.5. Kelvin pendant drop with repeated bulges. In 1886, Lord Kelvin proposed a geometric integration procedure that the quasistatic profile remains no long graph representation and becomes “repeated bulges” when the height of the pendant drop exceeds a critical height u_c . To compute the “repeated bulges”, which certainly break the vertical single graph representation setting, we will first describe the droplet using inverse function $X(u)$ (in horizontal graph setting) and give the gradient flow formulation in terms of $X(u)$. By solving the DAEs for $X(u)$ with $\kappa < 0$, which describes the quasi-static dynamics of a pendant droplet, we will recover multiple interfacial shape including lightbulb, hourglass shapes with different bond numbers. We refer to [30] for simulations and stability analysis of a liquid drop in hydrostatic states.

For the case the capillary surface can not be expressed uniquely by the graph function $u(x)$, we use the horizontal graph setting suggested by the inverse function $X(u)$. Assume there is only one maximum, denoted as u_m , for the height of the quasi-static profile $u(x)$ of the droplet. In the following derivation for the dynamic system, we always assume there is only one maximum for $u(x)$, which is indeed correct for the quasi-static dynamics of a pendant droplet (see (C.16)). Therefore for the right part of the droplet, i.e. from maximal point x_m such that $u(x_m) = u_m$ to the right end point, $u(x)$ is injective and thus revertible. In the following we only consider the right part of the droplet while the left part of the droplet can be handled by the same method. For simplicity, we assume the maximal point is $u(0) = u_m$ and assume the droplet is axially symmetric (see also the symmetric arguments in Section 4.1.1). Now we use the inverse function

$$(4.38) \quad X(u) := \{X; u(X) = u\}$$

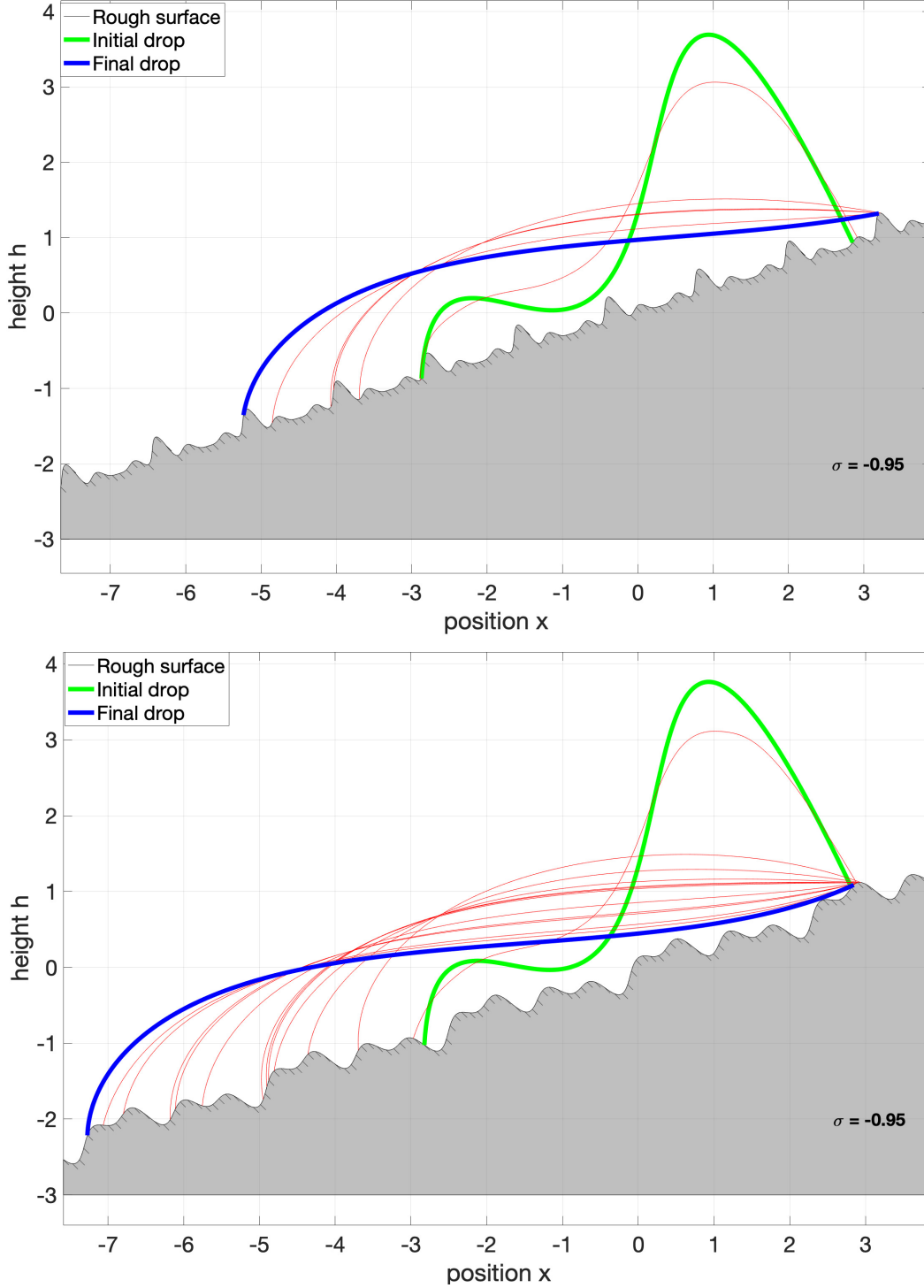


FIGURE 4. Evolution of a partially wetting droplet on inclined rough surfaces at equal time intervals using the second order time-space scheme in Section 3.2.3. Parameters: $\kappa = 0.3$, $\beta = 0.3$, number of moving grids in drop $N = 1000$, time step $\Delta t = 0.08$, initial drop profile $h(x, t)$ in (4.37) with initial endpoints $a(0) = -3, b(0) = 3$, final time $T = 96$, relative adhesion coefficient $\sigma = -0.95$, inclined effective angle $\theta_0 = 0.3$. (upper) Contact angle hysteresis on rough surface $w(x) = A(\sin(kx) + \cos(2kx))^2$, $A = 0.08$, $k = 5$, Bond number $\text{Bo} = 0.7108$. (lower) Contact angle hysteresis on rough surface $w(x) = A(\sin(kx) + \sin(kx/2) + \cos(2kx))$, $A = 1$, $k = 5$, Bond number $\text{Bo} = 0.7459$.

to identify the droplet on the right of its maximum $X = 0$

$$A := \{(u, x); 0 \leq u \leq u_m, 0 \leq x \leq X(u)\}.$$

Next we give the following governing equations for a 2D droplet in terms of $X(u)$, which can be derived similarly using a gradient flow on a Hilbert manifold

$$(4.39) \quad \begin{aligned} \beta \frac{\partial_t X}{\sqrt{1 + X_u^2}} &= \partial_u \left(\frac{X_u}{\sqrt{1 + X_u^2}} \right) - \kappa u + \lambda, \\ X(u_m) &= 0, \quad X_u(u_m) = -\infty, \\ \partial_t X(0, t) &= \frac{X_u}{\sqrt{1 + X_u^2}} \Big|_{u=0} - \sigma, \\ \int_0^{u_m} X(u) \, du &= V/2. \end{aligned}$$

The derivation is given in Appendix C for completeness.

To compute the Kelvin pendant droplet problem, we consider the quasi-static dynamics by taking $\beta = 0$ in (4.39). After desingularization, the quasi-static dynamics can be recast as the following DAEs for $(X(0, t), u_m(t), \theta(t), \lambda(t))$

$$(4.40) \quad \begin{aligned} \partial_t X(0, \cdot) &= -\cos \theta - \sigma, \\ J(u_m, \theta) &= 1, \\ X(0, \cdot) &= \frac{V}{2u_m} + \frac{1}{u_m} \int_0^{u_m} (u - u_m) \frac{-J(u, \theta)}{\sqrt{1 - J(u, \theta)^2}} \, du, \\ \frac{V}{2} &= \int_0^{\sqrt{u_m}} \frac{-2uJ(u, \theta)}{\sqrt{1 + J(u, \theta)}} \frac{\sqrt{u_m - u}}{\sqrt{1 - J(u, \theta)}} \, dw, \end{aligned}$$

where $J(u, \theta) := -\frac{\kappa u^2}{2} + \lambda u + \cos \theta$.

After solving $(X(0, t), u_m(t), \theta(t), \lambda(t))$ from the above DAEs, we can further compute the formula for $X(u, t)$

$$(4.41) \quad X(u, \cdot) = \int_u^{u_m} \frac{J(u, \theta)}{\sqrt{1 - J(u)^2}} \, du.$$

We use the DAEs solver *ode15s* in Matlab to solve the solution to DAEs (4.40) with the initial data

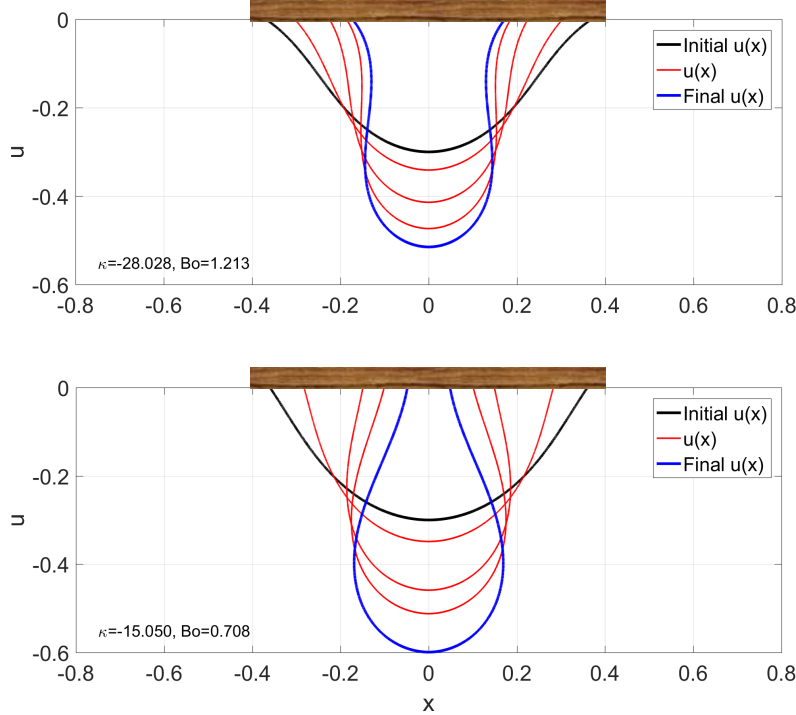
$$(4.42) \quad \theta_{in} = \frac{3\pi}{16}, \quad u_m(0) = 0.3$$

and the final Young's angle $\theta_f = \frac{2.7\pi}{8}$. The parameters in DAEs (4.40) are

$$(4.43) \quad \kappa = -28.028, \quad \sigma = -\cos(\theta_f).$$

With $u_m(0) = 0.3$, we start the DAEs by first solving the initial data $b(0)$ and $\lambda(0)$ from (4.40). The final time in *ode15s* is $T = 4$. We have $b(0) = 0.3704539$, $b(4) = 0.17438388$. The corresponding Bond number is $\text{Bo} = 1.213$. The final bulge shape of the pendant droplet (blue line) at $T = 4$ is illustrated in (upper) Fig. 5.

FIGURE 5. Kelvin pendant droplets. The evolution of pendant droplets at equal time intervals are computed using DAEs (4.40) with initial data $u_m(0) = 0.3$ and final time $T = 4$. The upper figure has an initial angle $\theta_{in} = \frac{3\pi}{16}$, final Young's angle $\theta_f = \frac{2.7\pi}{8}$ and the physical parameters $\kappa = -28.028, \text{Bo} = 1.213$. The lower figure has an initial angle $\theta_{in} = \frac{5\pi}{16}$, final Young's angle $\theta_f = \frac{4.7\pi}{8}$ and the physical parameters $\kappa = -15.0, \text{Bo} = 0.708$.



Next we take different parameters with a non-wetting Young's angle. The initial data is

$$(4.44) \quad \theta_{in} = \frac{5\pi}{16}, \quad u_m(0) = 0.3.$$

and final Young's angle is $\theta_f = \frac{4.7\pi}{8}$. The parameters in DAEs (4.40) are

$$(4.45) \quad \kappa = -15.05, \quad \sigma = -\cos(\theta_f),$$

With $u_m(0) = 0.3$, we start the DAEs by first solving the initial data $b(0)$ and $\lambda(0)$ from (4.40). The corresponding Bond number is $\text{Bo} = 0.708$. The final time in *ode15s* is $T = 4$. We have $b(0) = 0.3617157, b(4) = 0.05020375$. The final lightbulb shape of the pendant droplet (blue line) at $T = 4$ is illustrated in (lower) Fig. 5.

ACKNOWLEDGE

The authors wish to thank Professor Thomas Witelski for some valuable discussions. J.-G. Liu was supported in part by the National Science Foundation (NSF) under award DMS-1812573 and the NSF grant RNMS-1107444 (KI-Net).

REFERENCES

- [1] *Macroscopic and Large Scale Phenomena: Coarse Graining, Mean Field Limits and Ergodicity*, volume 3 of *Lecture Notes in Applied Mathematics and Mechanics*. Springer International Publishing, 2016.
- [2] Giovanni Alberti and Antonio DeSimone. Quasistatic evolution of sessile drops and contact angle hysteresis. *Archive for Rational Mechanics and Analysis*, 202(1):295348, Oct 2011.
- [3] Luigi Ambrosio, Nicola Gigli, and Giuseppe Savar. *Gradient flows: in metric spaces and in the space of probability measures*. Lectures in mathematics ETH Zrich. Birkhuser, 2005.
- [4] L. A. Caffarelli and A. Mellet. Capillary drops: Contact angle hysteresis and sticking drops. *Calculus of Variations and Partial Differential Equations*, 29(2):141160, Mar 2007.
- [5] L. A. Caffarelli and A. Mellet. *Capillary drops on an inhomogeneous surface*, volume 446, page 175201. American Mathematical Society, 2007.
- [6] Luis Caffarelli and Sandro Salsa. *A Geometric Approach to Free Boundary Problems*, volume 68 of *Graduate Studies in Mathematics*. American Mathematical Society, Jun 2005.
- [7] Luis A Caffarelli, K-A Lee, and Antoine Mellet. Homogenization and flame propagation in periodic excitable media: the asymptotic speed of propagation. *Communications on Pure and Applied Mathematics: A Journal Issued by the Courant Institute of Mathematical Sciences*, 59(4):501–525, 2006.
- [8] Xinfu Chen, Xiao-Ping Wang, and Xianmin Xu. Effective contact angle for rough boundary. *Physica D: Nonlinear Phenomena*, 242(1):5464, Jan 2013.
- [9] Stephen H. Davis. Moving contact lines and rivulet instabilities. part 1. the static rivulet. *Journal of Fluid Mechanics*, 98(2):225242, May 1980.
- [10] P. G. de Gennes. Wetting: statics and dynamics. *Reviews of Modern Physics*, 57(3):827863, Jul 1985.
- [11] Pierre-Gilles De Gennes, Françoise Brochard-Wyart, and David Quéré. *Capillarity and wetting phenomena: drops, bubbles, pearls, waves*. Springer Science & Business Media, 2013.
- [12] Masao Doi. *Soft matter physics*. Oxford University Press, 2013.
- [13] Selim Esedoglu, Richard Tsai, and Steven Ruuth. Threshold dynamics for high order geometric motions. *Interfaces and Free Boundaries*, page 263282, 2008.
- [14] Selim Esedo Lu and Felix Otto. Threshold dynamics for networks with arbitrary surface tensions. *Communications on Pure and Applied Mathematics*, 68(5):808864, May 2015.
- [15] William M. Feldman. Stability of serrins problem and dynamic stability of a model for contact angle motion. *SIAM Journal on Mathematical Analysis*, 50(3):33033326, Jan 2018.
- [16] William M. Feldman and Inwon C. Kim. Dynamic Stability of Equilibrium Capillary Drops. *Arch Rational Mech Anal*, 211(3):819–878, March 2014.
- [17] William M. Feldman and Inwon C. Kim. Liquid drops on a rough surface. *Communications on Pure and Applied Mathematics*, 71(12):24292499, Dec 2018.
- [18] Robert Finn and Marvin Shinbrot. The capillary contact angle, ii: The inclined plane. *Mathematical Methods in the Applied Sciences*, 10(2):165196, May 1988.
- [19] Alexandre Freire. Mean curvature motion of graphs with constant contact angle at a free boundary. *Analysis & PDE*, 3(4):359407, Sep 2010.
- [20] Min Gao and Xiao-Ping Wang. A gradient stable scheme for a phase field model for the moving contact line problem. *Journal of Computational Physics*, 231(4):1372 – 1386, 2012.
- [21] Yoshikazu Giga. *Surface evolution equations: a level set approach*. Monographs in mathematics. Birkhuser Verlag, 2006.
- [22] Natalie Grunewald and Inwon Kim. A variational approach to a quasi-static droplet model. *Calculus of Variations and Partial Differential Equations*, 41(12):119, May 2011.
- [23] Wei Jiang, Weizhu Bao, Carl V. Thompson, and David J. Srolovitz. Phase field approach for simulating solid-state dewetting problems. *Acta Materialia*, 60(15):55785592, Sep 2012.
- [24] Inwon Kim and Antoine Mellet. Liquid drops sliding down an inclined plane. *Transactions of the American Mathematical Society*, 366(11):61196150, May 2014.

- [25] Ming-Chih Lai, Yu-Hau Tseng, Huaxiong Huang, et al. Numerical simulation of moving contact lines with surfactant by immersed boundary method. *Communications in Computational Physics*, 8(4):735, 2010.
- [26] Shingyu Leung and Hongkai Zhao. A grid based particle method for moving interface problems. *Journal of Computational Physics*, 228(8):29933024, May 2009.
- [27] Alexander Mielke and Tom Roubiek. *Rate-independent systems: theory and application*. Applied mathematical sciences. Springer, 2015.
- [28] L. W. Morland. A fixed domain method for diffusion with a moving boundary. *Journal of Engineering Mathematics*, 16(3):259269, Sep 1982.
- [29] Klingenberg Wilhelm P.A. *Riemannian Geometry*. De Gruyter, 2011.
- [30] C. Pozrikidis. Stability of sessile and pendant liquid drops. *Journal of Engineering Mathematics*, 72(1):1–20, February 2012.
- [31] Tiezheng Qian, Xiao-Ping Wang, and Ping Sheng. A variational approach to moving contact line hydrodynamics. *Journal of Fluid Mechanics*, 564:333, Oct 2006.
- [32] R. M. S. M. Schulkes. The evolution and bifurcation of a pendant drop. *Journal of Fluid Mechanics*, 278:83100, Nov 1994.
- [33] Yi Sui, Hang Ding, and Peter D.M. Spelt. Numerical simulations of flows with moving contact lines. *Annual Review of Fluid Mechanics*, 46(1):97119, Jan 2014.
- [34] Dong Wang, Xiao-Ping Wang, and Xianmin Xu. An improved threshold dynamics method for wetting dynamics. *Journal of Computational Physics*, 392:291310, Sep 2019.
- [35] Yan Wang, Wei Jiang, Weizhu Bao, and Dave J. Srolovitz. Sharp interface model for solid-state dewetting problems with weakly anisotropic surface energies. *Physical Review B*, 91(4):045303, Jan 2015. arXiv: 1407.8331.
- [36] Jian-Jun Xu and Weiqing Ren. A level-set method for two-phase flows with moving contact line and insoluble surfactant. *Journal of Computational Physics*, 263:71–90, 2014.
- [37] Xianmin Xu, Yana Di, and Masao Doi. Variational method for contact line problems in sliding liquids. *Phys. Fluids*, 28:087101, 2016.
- [38] Kensuke Yokoi, Damien Vadillo, John Hinch, and Ian Hutchings. Numerical studies of the influence of the dynamic contact angle on a droplet impacting on a dry surface. *Physics of Fluids*, 21(7):072102, Jul 2009.
- [39] Thomas Young. iii, an essay on the cohesion of fluids. *Philosophical transactions of the royal society of London*, (95):65–87, 1805.
- [40] Hong-Kai Zhao, T. Chan, B. Merriman, and S. Osher. A variational level set approach to multiphase motion. *Journal of Computational Physics*, 127(1):179195, Aug 1996.

APPENDIX A. PROOF FOR THE TRUNCATION ANALYSIS OF FIRST AND SECOND ORDER SCHEMES

In this section, we give some truncation error estimates for the first and second order schemes in the case $w(x) = 0$, $\theta_0 = 0$ and thus $h(x) = u(x)$. Now the governing equation (2.39) becomes

$$\begin{aligned}
 \beta \frac{\partial_t u(x, t)}{\sqrt{1 + (\partial_x u)^2}} &= \frac{\partial}{\partial x} \left(\frac{\partial_x u}{\sqrt{1 + (\partial_x u)^2}} \right) - \kappa u + \lambda(t), \quad x \in (a(t), b(t)), \\
 u(a(t), t) &= u(b(t), t) = 0, \\
 a'(t) &= \sigma + \frac{1}{\sqrt{1 + (\partial_x u)^2}}, \quad x = a(t), \\
 b'(t) &= -\sigma - \frac{1}{\sqrt{1 + (\partial_x u)^2}}, \quad x = b(t), \\
 \int_{a(t)}^{b(t)} u(x, t) dx &= V.
 \end{aligned}
 \tag{A.1}$$

Proof of Lemma 3.1 (first order truncation error estimates). Let $a(t^{n+1}), b(t^{n+1}), u(x^{n+1}, t^{n+1})$ for $x^{n+1} \in [a(t^{n+1}), b(t^{n+1})]$ be the exact solution to (A.1) evaluated at $t = t^{n+1}$ with initial data at $t = t^n$, $a^n, b^n, u^n(x^n)$ for $x^n \in [a^n, b^n]$. We outline the idea of proof below.

Step 1. Truncation error estimate (3.9) for moving boundary. By Taylor expansion

$$(A.2) \quad a(t^{n+1}) = a^n + a'(t^n)\Delta t + O(\Delta t^2),$$

and the boundary condition in (A.1),

$$(A.3) \quad a'(t^n) = \left(\sigma + \frac{1}{\sqrt{1 + (\partial_x u^n)^2}} \right) \Big|_{a^n},$$

we have

$$(A.4) \quad a(t^{n+1}) = a^n + \Delta t \left(\sigma + \frac{1}{\sqrt{1 + (\partial_x u^n)^2}} \right) \Big|_{a^n} + O(\Delta t^2).$$

Similarly for $b(t^{n+1})$, we also have

$$(A.5) \quad b(t^{n+1}) = b^n - \Delta t \left(\sigma + \frac{1}{\sqrt{1 + (\partial_x u^n)^2}} \right) \Big|_{b^n} + O(\Delta t^2).$$

Next, we prove truncation error estimate (3.10) and divide the proof into four steps.

Step 2. Map the moving domain to fixed domain. We map the moving domain $[a(t), b(t)]$ to the fixed domain $[0, 1]$ by $Z(x, t) = \frac{x-a(t)}{b(t)-a(t)} \in [0, 1]$ for any $x \in [a(t), b(t)]$. Particularly, at different times we have the relation

$$(A.6) \quad Z(x^{n+1}, t^{n+1}) = Z(x^n, t^n) = Z(x^{n-1}, t^{n-1}) = Z(x^{n+\frac{1}{2}}, t^{n+\frac{1}{2}})$$

for independent variables $x^k \in [a^k, b^k]$, $k = n-1, n, n+\frac{1}{2}, n+1$ respectively.

Denote $U(Z, t) := u(x, t)$. Then changing of variables shows that

$$(A.7) \quad \partial_t u = \partial_t U + \partial_Z U \partial_t Z, \quad \partial_x u = \frac{1}{b-a} \frac{\partial U}{\partial Z}.$$

Then we recast (A.1) in terms of Z, U variables

$$(A.8) \quad \frac{\beta}{\sqrt{1 + (\frac{\partial_z U}{b-a})^2}} (\partial_t U + \partial_Z U \partial_t Z) = \frac{1}{(b-a)^2} \partial_z \left(\frac{\partial_z U}{\sqrt{1 + (\frac{\partial_z U}{b-a})^2}} \right) - \kappa U + \lambda.$$

Step 3. Truncation error for the term $\partial_t u = \partial_t U + \partial_Z U \partial_t Z$. First, using the backward Euler approximation, we can approximate this term. From relation (A.6), we have for $x^{n+1} \in [a(t^{n+1}), b(t^{n+1})]$,

$$(A.9) \quad \begin{aligned} \partial_t u(x^{n+1}, t^{n+1}) &= \partial_t U(Z, t^{n+1}) + \partial_Z U(Z, t^{n+1}) \partial_t Z(x^{n+1}, t^{n+1}) \\ &= \frac{U(Z, t^{n+1}) - U^n(Z)}{\Delta t} + \partial_Z U^n(Z) \frac{Z(x^{n+1}, t^{n+1}) - Z(x^{n+1}, t^n)}{\Delta t} + O(\Delta t) \\ &= \frac{u(x^{n+1}, t^{n+1}) - u^n(x^n)}{\Delta t} + \partial_x u^n(x^n) \frac{\partial x^n}{\partial Z} \frac{Z(x^n, t^n) - Z(x^{n+1}, t^n)}{\Delta t} + O(\Delta t) \\ &= \frac{u(x^{n+1}, t^{n+1}) - u^n(x^n)}{\Delta t} + \frac{\partial_x u^n(x^n)(x^n - x^{n+1})}{\Delta t} + O(\Delta t), \end{aligned}$$

where

$$(A.10) \quad x^n = a^n + \frac{b^n - a^n}{b(t^{n+1}) - a(t^{n+1})} (x^{n+1} - a(t^{n+1})).$$

Denote

$$(A.11) \quad u^*(x^{n+1}, t^n) := u^n(x^n) + \partial_x u^n(x^n)(x^{n+1} - x^n),$$

which is exactly (3.3).

In summary, the semi-Lagrangian term has first order accuracy

$$(A.12) \quad \partial_t u(x^{n+1}, t^{n+1}) = \frac{u(x^{n+1}, t^{n+1}) - u^*(x^{n+1}, t^n)}{\Delta t} + O(\Delta t).$$

Step 4. Truncation error for the stretching term $\frac{1}{\sqrt{1+(\partial_x u)^2}}$. From the relation between x^n and x^{n+1} in (A.10) and the truncation error in Step 1, we have

$$\begin{aligned} x^{n+1} - x^n &= \frac{(b^{n+1} - b^n) - (a^{n+1} - a^n)}{b^{n+1} - a^{n+1}} x^{n+1} + \frac{(b^n - a^n)a^{n+1} - (b^{n+1} - a^{n+1})a^n}{b^{n+1} - a^{n+1}} \\ &= \frac{(b^{n+1} - b^n) - (a^{n+1} - a^n)}{b^{n+1} - a^{n+1}} x^{n+1} + \frac{b^n(a^{n+1} - a^n) - a^n(b^{n+1} - b^n)}{b^{n+1} - a^{n+1}} \\ &= O(b^{n+1} - b^n) + O(a^{n+1} - a^n) \end{aligned}$$

and thus

$$(A.13) \quad |x^{n+1} - x^n| = O(\Delta t).$$

Combing (A.10) and (A.11), we have

$$(A.14) \quad \begin{aligned} \partial_x u^*(x^{n+1}, t^n) &= \partial_x u^n(x^n) \frac{\partial x^n}{\partial x^{n+1}} + \partial_x u^n(x^n) \partial_x (x^{n+1} - x^n) + \partial_{xx} u^n(x^n) \frac{\partial x^n}{\partial x^{n+1}} (x^{n+1} - x^n) \\ &= \partial_x u^n(x^n) \frac{b^n - a^n}{b(t^{n+1}) - a(t^{n+1})} + \partial_x u^n(x^n) \frac{(b(t^{n+1}) - b^n) - (a(t^{n+1}) - a^n)}{b(t^{n+1}) - a(t^{n+1})} + O(|x^{n+1} - x^n|) \\ &= \partial_x u^n(x^n) + O(|x^{n+1} - x^n|). \end{aligned}$$

In summary, we have

$$(A.15) \quad \frac{1}{b(t^{n+1}) - a(t^{n+1})} \partial_z U^{n*}(Z) = \partial_x u^*(x^{n+1}, t^n) = \partial_x u^n(x^n) + O(\Delta t) = \frac{1}{b^n - a^n} \partial_z U^n(Z) + O(\Delta t).$$

Step 5. Truncation error for $u(x^{n+1}, t^{n+1})$, $x^{n+1} \in [a(t^{n+1}), b(t^{n+1})]$. Plugging $u(x^{n+1}, t^{n+1})$ into the first equation in (A.1), from (A.12) and (A.15)

$$(A.16) \quad \frac{\beta}{\sqrt{1 + (\partial_x u^*(t^n))^2}} \frac{u(t^{n+1}) - u^*(t^n)}{\Delta t} = \partial_x \left(\frac{\partial_x u(t^{n+1})}{\sqrt{1 + (\partial_x u^*(t^n))^2}} \right) - \kappa u(t^{n+1}) + \lambda + O(\Delta t),$$

for $x^{n+1} \in [a(t^{n+1}), b(t^{n+1})]$. We conclude the proof. \square

Proof of Lemma 3.2 (second order truncation error estimates). Let $a(t^{n+1}), b(t^{n+1}), u(x^{n+1}, t^{n+1})$ for $x^{n+1} \in [a(t^{n+1}), b(t^{n+1})]$ be the exact solution to (A.1) evaluated at $t = t^{n+1}$ with initial data at $t = t^n$, $a^n, b^n, u^n(x^n)$ for $x^n \in [a^n, b^n]$. We will prove truncation error estimates (3.25) and (3.26) separately in Step 1 and Step 2. We outline the idea of proof below.

Step 1. Second order truncation error for the moving boundary (3.25).

We first illustrate the idea of the usual truncation error estimates for the predictor-corrector ODE solver for $v' = f(v)$ with $v'' = f'(v)f(v)$. By Taylor expansion,

$$\begin{aligned}
v^{n+1} &= v^n + \Delta t f(v^n) + \frac{(\Delta t)^2}{2} f(v^n) f'(v^n) + O(\Delta t^3) \\
\text{(A.17)} \quad &= v^n + \frac{\Delta t}{2} [f(v^n) + f(v^n) + \Delta t f(v^n) f'(v^n)] + O(\Delta t^3) \\
&= v^n + \frac{\Delta t}{2} [f(v^n) + f(v^n + \Delta t f(v^n))] + O(\Delta t^3),
\end{aligned}$$

which is equivalent to

$$\text{(A.18)} \quad \frac{\tilde{v}^{n+1} - v^n}{\Delta t} = f(v^n), \quad \frac{v^{n+1} - v^n}{\Delta t} = \frac{1}{2} [f(v^n) + f(\tilde{v}^{n+1})] + O(\Delta t^2).$$

Moreover, for any smooth function $w(v)$, we have the second order estimate

$$\text{(A.19)} \quad w(v(t^{n+\frac{1}{2}})) = \frac{1}{2} (w(v^n) + w(\tilde{v}^{n+1})) + O(\Delta t^2).$$

Indeed, since $v(t^{n+\frac{1}{2}}) = v^n + \frac{\Delta t}{2} f(v^n) + O(\Delta t^2)$, by Taylor's expansion we have

$$\text{(A.20)} \quad \text{LHS} = w(v^n) + \frac{\Delta t}{2} w'(v^n) f(v^n) + O(\Delta t^2) = \frac{1}{2} [w(v^n) + w(v^n + \Delta t f(v^n))] + O(\Delta t^2) = \text{RHS}.$$

(A.19) also gives another method for second order truncation error estimate by evaluating the equation $v' = f(v)$ at $t^{n+\frac{1}{2}}$, which is (A.18). The truncation error in Step 2 will rely on this method.

Second, we again recast the equation for the moving boundary in terms of the fixed domain variable $U(Z, t) = u(x, t)$ with $Z(x, t) = \frac{x-a(t)}{b(t)-a(t)} \in [0, 1]$.

$$\begin{aligned}
\text{(A.21)} \quad a'(t) &= \sigma + \frac{1}{\sqrt{1 + \frac{(\partial_z U)^2|_{Z=0}}{(b(t)-a(t))^2}}} =: g(a(t), b(t), \partial_z U(0, t)), \\
b'(t) &= -\sigma - \frac{1}{\sqrt{1 + \frac{(\partial_z U)^2|_{Z=1}}{(b(t)-a(t))^2}}} =: q(a(t), b(t), \partial_z U(1, t)).
\end{aligned}$$

Third, analogue to the usual predictor-corrector ODE solver, we calculate the truncation error for a^{n+1} . Notice

$$\text{(A.22)} \quad a''(t) = a' \partial_1 g + b' \partial_2 g + \partial_3 g \partial_{tz} U|_{Z=0}.$$

Taylor's expansion gives us

$$a(t^{n+1}) = a^n + \Delta t g(a^n, b^n, \partial_z U^n) + \frac{\Delta t^2}{2} [a' \partial_1 g + b' \partial_2 g + \partial_3 g \partial_{tz} U|_{Z=0}]^n + O(\Delta t^3).$$

Hence from Taylor's expansion of $g(\tilde{a}^{n+1}, \tilde{b}^{n+1}, \partial_z \tilde{U}^{n+1})$

$$\begin{aligned}
\text{(A.23)} \quad &\frac{a(t^{n+1}) - a^n}{\Delta t} \\
&= \frac{1}{2} g(a^n, b^n, \partial_z U^n) + \frac{1}{2} g\left(a^n + \Delta t \frac{\tilde{a}^{n+1} - a^n}{\Delta t}, b^n + \Delta t \frac{\tilde{b}^{n+1} - b^n}{\Delta t}, \partial_z U^n + \Delta t \frac{\partial_z \tilde{U}^{n+1} - \partial_z U^n}{\Delta t}\right) + O(\Delta t^2) \\
&= \frac{1}{2} g(a^n, b^n, \partial_z U^n) + \frac{1}{2} g(\tilde{a}^{n+1}, \tilde{b}^{n+1}, \partial_z \tilde{U}^{n+1}) + O(\Delta t^2),
\end{aligned}$$

provided $\frac{\tilde{a}^{n+1}-a^n}{\Delta t} - (a')^n$ and $\frac{\partial_z \tilde{U}^{n+1}-\partial_z U^n}{\Delta t} - (\partial_{zt}U)^n|_{z=0}$ has $O(\Delta t)$ accuracy.

Finally, we prove $\frac{\tilde{a}^{n+1}-a^n}{\Delta t} - (a')^n$ and $\frac{\partial_z \tilde{U}^{n+1}-\partial_z U^n}{\Delta t} - (\partial_{zt}U)^n|_{z=0}$ has $O(\Delta t)$ accuracy. Since the predictor \tilde{a}^{n+1} is given by the first order scheme in Section 3.1, we know $\frac{\tilde{a}^{n+1}-a^n}{\Delta t} - (a')^n$ has $O(\Delta t)$ accuracy and we obtain (3.9). To estimate $\frac{\partial_z \tilde{U}^{n+1}-\partial_z U^n}{\Delta t}$, we give the following claim.

Claim 1: Assume we have the error estimates

$$(A.24) \quad \tilde{a}^{n+1} - a^{n+1} = O(\Delta t^2), \quad \tilde{b}^{n+1} - b^{n+1} = O(\Delta t^2), \quad \tilde{u}^{n+1}(\tilde{x}^{n+1}) - u^{n+1}(x^{n+1}) = O(\Delta t^2).$$

Then we have the second order accuracy

$$(A.25) \quad (\partial_x \tilde{u})^{n+1}(\tilde{x}^{n+1}) = (\partial_x u)^{n+1}(x^{n+1}) + O(\Delta t^2).$$

The proof of Claim 1 is based on changing moving domain to fixed domain by $Z = \frac{\tilde{x}^{n+1}-\tilde{a}^{n+1}}{\tilde{b}^{n+1}-\tilde{a}^{n+1}} = \frac{x^{n+1}-a^{n+1}}{b^{n+1}-a^{n+1}}$, which is similar to (A.21) and will be omitted. Notice the first order accuracy of predictor \tilde{a}^{n+1} , \tilde{b}^{n+1} and we used implicit elliptic solver with second order accuracy in (3.22) for predictor \tilde{u}^{n+1} , so the assumptions in claim 1 are satisfied automatically. Thus from the Taylor expansion and claim 1 we know

$$(A.26) \quad \frac{\partial_z \tilde{U}^{n+1} - \partial_z U^n}{\Delta t} + O(\Delta t) = \frac{\partial_z U^{n+1} - \partial_z U^n}{\Delta t} + O(\Delta t) = (\partial_{tz}U)^n + O(\Delta t).$$

Therefore, we complete the second order truncation error estimates for the moving boundary (3.25).

Step 2. Second order truncation error estimates (3.26) for u^{n+1} .

First from the similar argument for (A.19), we have the following generalized claim

Claim 2: For any smooth function $w(v(x, t), v_x(x, t), v_{xx}(x, t), x, t)$, we have

$$(A.27) \quad \begin{aligned} & w(v(t^{n+\frac{1}{2}}), v_x(t^{n+\frac{1}{2}}), v_{xx}(t^{n+\frac{1}{2}}), x^{n+\frac{1}{2}}, t^{n+\frac{1}{2}}) \\ &= \frac{1}{2} [w(v^n, v_x^n, v_{xx}^n, x^n, t^n) + w(v^{n+1}, v_x^{n+1}, v_{xx}^{n+1}, x^{n+1}, t^{n+1})] + O(\Delta t^2), \end{aligned}$$

where the equality holds in the sense of changing variables to fixed domain $Z = \frac{x-a(t)}{b(t)-a(t)}$ with the relation (A.6).

Second, notice the derivation for the term $\partial_t h$ in (3.21) gives the second order accuracy

$$\frac{u^{n+1}(x^{n+1}) - \tilde{u}^{n*}}{\Delta t} = \partial_t u(x^{n+\frac{1}{2}}, t^{n+\frac{1}{2}}) + O(\Delta t^2).$$

Using further Claim 1 and Claim 2, we obtain the second order accuracy for (3.26).

$$\begin{aligned} & \frac{1}{2} \left[\frac{1}{\sqrt{1 + (\partial_x u^n)^2}} + \frac{1}{\sqrt{1 + (\partial_x \tilde{u}^{n+1})^2}} \right] = \frac{1}{\sqrt{1 + (\partial_x u)^2}} \Big|_{t^{n+\frac{1}{2}}} + O(\Delta t^2), \\ & \frac{1}{2} \frac{\partial}{\partial x} \left(\frac{\partial_x u^{n+1}}{\sqrt{1 + (\partial_x \tilde{u}^{n+1})^2}} + \frac{\partial_x u^n}{\sqrt{1 + (\partial_x u^n)^2}} \right) = \frac{\partial}{\partial x} \left(\frac{\partial_x u^{n+1}}{\sqrt{1 + (\partial_x u^{n+1})^2}} \right) \Big|_{t^{n+\frac{1}{2}}} + O(\Delta t^2), \end{aligned}$$

Therefore, we complete the second order truncation error estimates for (3.26). \square

APPENDIX B. PSEUDO-CODES FOR FIRST AND SECOND ORDER SCHEMES

B.1. First order in time and second order in space. We present a pseudo-code for the first order scheme in Section 3.1.1:

1. Grid for time: $t^n = n\Delta t$, $n = 0, 1, \dots$, where Δt is time step.
2. Moving grid for space: Fix N and denote $\tau^n = \frac{b^n - a^n}{N}$ as spatial step size.

$$(B.1) \quad x_j^n = a^n + j\tau^n, \quad j = -1, 0, 1, \dots, N + 1.$$

3. Denote $u_j^n \approx u(x_j^n, t^n)$ with $u_0^n = u_N^n = 0$.
4. Calculate $V := \sum_{j=1}^{N-1} u_j^0 \tau^0$.
5. Update a^{n+1}, b^{n+1} , $j = 0, 1, \dots, N$.

$$(B.2) \quad \frac{a^{n+1} - a^n}{\Delta t} = \sigma \sqrt{1 + (\partial_x w)_0^2} + \frac{1 + (\partial_x h^n)_0 (\partial_x w)_0}{\sqrt{1 + (\partial_x h^n)_0^2}},$$

with $(\partial_x w)_0 = \partial_x w(x_0^n)$, $(\partial_x h^n)_0 = \frac{4h_1^n - h_2^n - 3h_0^n}{2\tau^n}$.

$$(B.3) \quad \frac{b^{n+1} - b^n}{\Delta t} = -\sigma \sqrt{1 + (\partial_x w)_N^2} - \frac{1 + (\partial_x h^n)_N (\partial_x w)_N}{\sqrt{1 + (\partial_x h^n)_N^2}},$$

with $(\partial_x w)_N = \partial_x w(x_N^n)$, $(\partial_x h^n)_N = \frac{-4h_{N-1}^n + h_{N-2}^n + 3h_N^n}{2\tau^n}$.

5. Update the moving grids

$$x_j^{n+1} = a^{n+1} + j\tau^{n+1}, \quad j = 0, 1, \dots, N, \quad \tau^{n+1} = \frac{b^{n+1} - a^{n+1}}{N}.$$

5. From (3.3),

$$h_j^{n*} = h_j^n + \frac{h_{j+1}^n - h_{j-1}^n}{2\tau^n} (a^{n+1} - a^n + j(\tau^{n+1} - \tau^n)), \quad j = 1, \dots, N - 1;$$

$$h_0^{n*} = w(x_0^n) + \frac{4h_1^n - h_2^n - 3h_0^n}{2\tau^n} (a^{n+1} - a^n), \quad h_N^{n*} = w(x_N^n) + \frac{-4h_{N-1}^n + h_{N-2}^n + 3h_N^n}{2\tau^n} (b^{n+1} - b^n).$$

6. Solve h^{n+1} semi-implicitly

For $j = 1, \dots, N-1$, with $h_0^{n+1} = w(x_0^{n+1})$, $h_N^{n+1} = w(x_N^{n+1})$,

$$(B.4) \quad \beta \frac{h_j^{n+1} - h_j^{n*}}{\Delta t} \frac{1}{\sqrt{1 + (\partial_x h_j^{n*})^2}}$$

$$= \frac{1}{(\tau^{n+1})^2} \left[\frac{h_{j+1}^{n+1} - h_j^{n+1}}{\sqrt{1 + (\partial_x h_{j+\frac{1}{2}}^{n*})^2}} - \frac{h_j^{n+1} - h_{j-1}^{n+1}}{\sqrt{1 + (\partial_x h_{j-\frac{1}{2}}^{n*})^2}} \right] - \kappa (h_j^{n+1} \cos \theta_0 + x_j^{n+1} \sin \theta_0) + \lambda^{n+1},$$

$$\sum_{j=1}^{N-1} (h_j^{n+1} - w(x_j^{n+1})) \tau^{n+1} = V,$$

where

$$(B.5) \quad \partial_x h_j^{n*} = \frac{h_{j+1}^{n*} - h_{j-1}^{n*}}{2\tau^{n+1}}, \quad \partial_x h_{j+\frac{1}{2}}^{n*} = \frac{h_{j+1}^{n*} - h_j^{n*}}{\tau^{n+1}}, \quad \partial_x h_{j-\frac{1}{2}}^{n*} = \frac{h_j^{n*} - h_{j-1}^{n*}}{\tau^{n+1}}.$$

Due to the $O(|x^{n+1} - x^n|) = O(\Delta t)$ accuracy for $\partial_x u^*$ and $\partial_x u^n(x^n)$ in (A.14), to ensure the stability in the implementation, we replace (B.5) by

$$(B.6) \quad \partial_x h_j^n = \frac{h_{j+1}^n - h_{j-1}^n}{2\tau^n}, \quad \partial_x h_{j+\frac{1}{2}}^n = \frac{h_{j+1}^n - h_j^n}{\tau^n}, \quad \partial_x h_{j-\frac{1}{2}}^n = \frac{h_j^n - h_{j-1}^n}{\tau^n}.$$

The resulted linear system $\bar{A}y = f$ has a non-singular matrix

$$(B.7) \quad \bar{A} = \begin{pmatrix} A & e \\ e^T & 0 \end{pmatrix}_{N \times N},$$

where $y^T = (h_1^{n+1}, \dots, h_{N-1}^{n+1}, -(\tau^{n+1})^2 \lambda^{n+1})$, A is a diagonal-dominated tridiagonal matrix defined below, and $e^T = (1, \dots, 1) \in \mathbb{R}^{N-1}$. Denote $A_{(N-1) \times (N-1)} = (a_{ij})$ with

$$(B.8) \quad a_{j,j-1} = -\frac{1}{\sqrt{1 + (\partial_x h_{j-\frac{1}{2}}^n)^2}}, \quad a_{j,j+1} = -\frac{1}{\sqrt{1 + (\partial_x h_{j+\frac{1}{2}}^n)^2}}, \quad \alpha_j = \frac{\beta(\tau^{n+1})^2}{\Delta t \sqrt{1 + (\partial_x h_j^n)^2}}$$

$$a_{j,j} = -a_{j,j-1} - a_{j,j+1} + \alpha_j + \kappa \cos \theta_0 (\tau^{n+1})^2,$$

and (B.4) becomes for $j = 1, \dots, N-1$,

$$(B.9) \quad a_{j,j-1} h_{j-1}^{n+1} + a_{j,j} h_j^{n+1} + a_{j,j+1} h_{j+1}^{n+1} - (\tau^{n+1})^2 \lambda^{n+1} = \alpha_j h_j^{n*} - \kappa \sin \theta_0 x_j^{n+1} (\tau^{n+1})^2,$$

$$h_0^{n+1} = w(x_0^{n+1}), \quad h_N^{n+1} = w(x_N^{n+1}).$$

Notice we have a nonhomogeneous boundary condition so to impose the nonhomogeneous boundary condition for $j = 1, N-1$, we need to compute $a_{1,0} h_0^{n+1} = a_{1,0} w(x_0^{n+1})$, $a_{N-1,N} h_N^{n+1} = a_{N-1,N} w(x_N^{n+1})$ and move them to the right hand side.

B.2. Predictor-corrector scheme: second order in time and space. We present a pseudo-code for the second order scheme in Section 3.2.3:

1. Grid for time: $t^n = n\Delta t$, $n = 0, 1, \dots$, where Δt is time step.
2. Moving grid for space: Fix N and denote $\tau^n = \frac{b^n - a^n}{N}$ as spatial step size.

$$(B.10) \quad x_j^n = a^n + j\tau^n, \quad j = -1, 0, 1, \dots, N+1.$$

Denote $u_j^n \approx u(x_j^n, t^n)$ with $u_0^n = u_N^n = 0$.

3. Calculate $V := \sum_{j=1}^{N-1} u_j^0 \tau^0$.

4. Repeat the first order scheme (B.2), (B.3) in Section B.1 with implicit nonlinear elliptic solver. For $j = 1, \dots, N-1$, with $h_0^{n+1} = w(x_0^{n+1})$, $h_N^{n+1} = w(x_N^{n+1})$,

$$(B.11) \quad \beta \frac{h_j^{n+1} - h_j^{n*}}{\Delta t} \frac{1}{\sqrt{1 + (\partial_x h_j^{n+1})^2}}$$

$$= \frac{1}{(\tau^{n+1})^2} \left[\frac{h_{j+1}^{n+1} - h_j^{n+1}}{\sqrt{1 + (\partial_x h_{j+\frac{1}{2}}^{n+1})^2}} - \frac{h_j^{n+1} - h_{j-1}^{n+1}}{\sqrt{1 + (\partial_x h_{j-\frac{1}{2}}^{n+1})^2}} \right] - \kappa(h_j^{n+1} \cos \theta_0 + x_j^{n+1} \sin \theta_0) + \lambda^{n+1},$$

$$\sum_{j=1}^{N-1} (h_j^{n+1} - w(x_j^{n+1})) \tau^{n+1} = V,$$

where

$$\partial_x h_{j+\frac{1}{2}}^{n+1} := \frac{h_{j+1}^{n+1} - h_j^{n+1}}{\tau^{n+1}}, \quad \partial_x h_{j-\frac{1}{2}}^{n+1} = \frac{h_j^{n+1} - h_{j-1}^{n+1}}{\tau^{n+1}}.$$

Denote the results as the predictor $\tilde{a}^{n+1}, \tilde{b}^{n+1}, \tilde{h}^{n+1}(\tilde{x}^{n+1}), \tilde{\tau}^{n+1}$ for $\tilde{x}^{n+1} \in [\tilde{a}^{n+1}, \tilde{b}^{n+1}]$.

5. Update a^{n+1}, b^{n+1} , $j = 0, 1, \dots, N$.

$$\frac{a^{n+1} - a^n}{\Delta t} = \frac{1}{2} \left\{ \sigma \sqrt{1 + (\partial_x w)_0^2} + \sigma \sqrt{1 + (\partial_x \tilde{w})_0^2} + \frac{1 + (\partial_x h^n)_0 (\partial_x w)_0}{\sqrt{1 + (\partial_x h^n)_0^2}} + \frac{1 + (\partial_x \tilde{h}^{n+1})_0 (\partial_x \tilde{w})_0}{\sqrt{1 + (\partial_x \tilde{h}^{n+1})_0^2}} \right\},$$

$$\text{with } (\partial_x w)_0 := \partial_x w(x_0^n), \quad (\partial_x \tilde{w})_0 := \partial_x w(\tilde{x}_0^{n+1}),$$

$$\text{and } (\partial_x h^n)_0 := \frac{4h_1^n - h_2^n - 3h_0^n}{2\tau^n}, \quad (\partial_x \tilde{h}^{n+1})_0 := \frac{4\tilde{h}_1^{n+1} - \tilde{h}_2^{n+1} - 3\tilde{h}_0^{n+1}}{2\tilde{\tau}^{n+1}}.$$

$$\frac{b^{n+1} - b^n}{\Delta t} = -\frac{1}{2} \left\{ \sigma \sqrt{1 + (\partial_x w)_N^2} + \sigma \sqrt{1 + (\partial_x \tilde{w})_N^2} + \frac{1 + (\partial_x h^n)_N (\partial_x w)_N}{\sqrt{1 + (\partial_x h^n)_N^2}} + \frac{1 + (\partial_x \tilde{h}^{n+1})_N (\partial_x \tilde{w})_N}{\sqrt{1 + (\partial_x \tilde{h}^{n+1})_N^2}} \right\},$$

$$\text{with } (\partial_x w)_N := \partial_x w(x_N^n), \quad (\partial_x \tilde{w})_N := \partial_x w(\tilde{x}_N^{n+1}),$$

$$\text{and } (\partial_x h^n)_N := \frac{-4h_{N-1}^n - h_{N-2}^n - 3h_N^n}{2\tau^n}, \quad (\partial_x \tilde{h}^{n+1})_N := \frac{-4\tilde{h}_{N-1}^{n+1} + \tilde{h}_{N-2}^{n+1} + 3\tilde{h}_N^{n+1}}{2\tilde{\tau}^{n+1}}.$$

6. Update the moving grids

$$x_j^{n+1} = a^{n+1} + j\tau^{n+1}, \quad j = 0, 1, \dots, N, \quad \tau^{n+1} = \frac{b^{n+1} - a^{n+1}}{N}.$$

7. From (3.21), for $j = 1, \dots, N-1$

$$h_j^{n*} = h_j^n + \frac{1}{8} \left(\frac{1}{\tau^{n+1}} + \frac{1}{\tau^n} \right) (h_{j+1}^n - h_{j-1}^n + \tilde{h}_{j+1}^{n+1} - \tilde{h}_{j-1}^{n+1}) (a^{n+1} - a^n + j(\tau^{n+1} - \tau^n)),$$

$$h_0^{n*} = w(x_0^n) + \frac{1}{8} \left(\frac{1}{\tau^{n+1}} + \frac{1}{\tau^n} \right) [4h_1^n - h_2^n - 3h_0^n + 4\tilde{h}_1^{n+1} - \tilde{h}_2^{n+1} - 3\tilde{h}_0^{n+1}] (a^{n+1} - a^n),$$

$$h_N^{n*} = w(x_N^n) + \frac{1}{8} \left(\frac{1}{\tau^{n+1}} + \frac{1}{\tau^n} \right) [-4h_{N-1}^n + h_{N-2}^n - 3h_N^n - 4\tilde{h}_{N-1}^{n+1} + \tilde{h}_{N-2}^{n+1} + 3\tilde{h}_N^{n+1}] (b^{n+1} - b^n).$$

8. Solve h^{n+1} implicitly

For $j = 1, \dots, N-1$, with $h_0^{n+1} = w(x_0^{n+1})$, $h_N^{n+1} = w(x_N^{n+1})$,

(B.12)

$$\begin{aligned} & \beta \frac{h_j^{n+1} - h_j^{n*}}{\Delta t} \frac{1}{2} \left[\frac{1}{\sqrt{1 + (\partial_x h_j^n)^2}} + \frac{1}{\sqrt{1 + (\partial_x \tilde{h}_j^{n+1})^2}} \right] \\ &= \frac{1}{2(\tau^{n+1})^2} \left[\frac{h_{j+1}^{n+1} - h_j^{n+1}}{\sqrt{1 + (\partial_x \tilde{h}_{j+\frac{1}{2}}^{n+1})^2}} - \frac{h_j^{n+1} - h_{j-1}^{n+1}}{\sqrt{1 + (\partial_x \tilde{h}_{j-\frac{1}{2}}^{n+1})^2}} \right] + \frac{1}{2(\tau^n)^2} \left[\frac{h_{j+1}^n - h_j^n}{\sqrt{1 + (\partial_x h_{j+\frac{1}{2}}^n)^2}} - \frac{h_j^n - h_{j-1}^n}{\sqrt{1 + (\partial_x h_{j-\frac{1}{2}}^n)^2}} \right] \\ & \quad - \frac{\kappa}{2} [(h_j^{n+1} + h_j^n) \cos \theta_0 + (x_j^n + x_j^{n+1}) \sin \theta_0] + \lambda^{n+\frac{1}{2}}, \\ & \sum_{j=1}^{N-1} (h_j^{n+1} - w(x_j^{n+1})) \tau^{n+1} = V, \end{aligned}$$

where

$$\begin{aligned} \partial_x h_j^n &= \frac{h_{j+1}^n - h_{j-1}^n}{2\tau^n}, \quad \partial_x \tilde{h}_j^{n+1} = \frac{\tilde{h}_{j+1}^{n+1} - \tilde{h}_{j-1}^{n+1}}{2\tilde{\tau}^{n+1}} \\ \partial_x h_{j+\frac{1}{2}}^n &:= \frac{h_{j+1}^n - h_j^n}{\tau^n}, \quad \partial_x h_{j-\frac{1}{2}}^n = \frac{h_j^n - h_{j-1}^n}{\tau^n}, \quad \partial_x \tilde{h}_{j+\frac{1}{2}}^{n+1} := \frac{\tilde{h}_{j+1}^{n+1} - \tilde{h}_j^{n+1}}{\tilde{\tau}^{n+1}}, \quad \partial_x \tilde{h}_{j-\frac{1}{2}}^{n+1} = \frac{\tilde{h}_j^{n+1} - \tilde{h}_{j-1}^{n+1}}{\tilde{\tau}^{n+1}}. \end{aligned}$$

The resulted linear system $\bar{A}y = f$ has a matrix

$$(B.13) \quad \bar{A} = \begin{pmatrix} A & e \\ e^T & 0 \end{pmatrix}_{N \times N},$$

where A is a diagonal-dominated tridiagonal matrix defined below and $e^T = (1, \dots, 1) \in \mathbb{R}^{N-1}$.

Denote $A_{(N-1) \times (N-1)} = (a_{ij})$ with

(B.14)

$$\begin{aligned} a_{j,j-1} &= -\frac{1}{\sqrt{1 + (\partial_x \tilde{h}_{j-\frac{1}{2}}^{n+1})^2}}, \quad a_{j,j+1} = -\frac{1}{\sqrt{1 + (\partial_x \tilde{h}_{j+\frac{1}{2}}^{n+1})^2}}, \quad \alpha_j = \frac{\beta(\tau^{n+1})^2}{\Delta t} \left[\frac{1}{\sqrt{1 + (\partial_x h_j^n)^2}} + \frac{1}{\sqrt{1 + (\partial_x \tilde{h}_j^{n+1})^2}} \right] \\ a_{j,j} &= -a_{j,j-1} - a_{j,j+1} + \alpha_j + \kappa \cos \theta_0 (\tau^{n+1})^2, \end{aligned}$$

and (B.12) becomes for $j = 1, \dots, N-1$, $h_0^{n+1} = w(x_0^{n+1})$, $h_N^{n+1} = w(x_N^{n+1})$ and

(B.15)

$$\begin{aligned} & a_{j,j-1} h_{j-1}^{n+1} + a_{j,j} h_j^{n+1} + a_{j,j+1} h_{j+1}^{n+1} - (\tau^{n+1})^2 \lambda^{n+\frac{1}{2}} \\ &= \alpha_j h_j^{n*} - \kappa (\tau^{n+1})^2 [h_j^n \cos \theta_0 + \frac{x_j^{n+1} + x_j^n}{2} \sin \theta_0] + \frac{(\tau^{n+1})^2}{(\tau^n)^2} \left[\frac{h_{j+1}^n - h_j^n}{\sqrt{1 + (\partial_x h_{j+\frac{1}{2}}^n)^2}} - \frac{h_j^n - h_{j-1}^n}{\sqrt{1 + (\partial_x h_{j-\frac{1}{2}}^n)^2}} \right]. \end{aligned}$$

APPENDIX C. GRADIENT FLOW FOR HORIZONTAL GRAPH REPRESENTATION $X(u)$ AND DAES FOR QUASI-STATIC DYNAMICS

C.1. Gradient Flow for single sessile drop in non-wetting case: with volume constraint.

Recall the description of the non-wetting droplet in terms of $X(u)$ in (4.38). We consider the

manifold based on $X(u)$

$$(C.1) \quad \mathcal{M} := \{X(u) \in H^1(0, u_m); 0 \leq u \leq u_m, X(u_m) = 0, X_u(u_m) = -\infty\}.$$

Similar to Section 2, we calculate the gradient flow on manifold \mathcal{M} . Denote $\tilde{X}(u, s)$ with $\tilde{u}_m(s)$ are trajectory on \mathcal{M} starting from $X(u, t)$ with $u_m(t)$. Notice from $X(u_m(t), t) = 0$ we have

$$(C.2) \quad \partial_t \tilde{X} = -X_u \partial_t \tilde{u}_m \quad \text{for } u = u_m.$$

Consider the free energy

$$(C.3) \quad \begin{aligned} \frac{1}{2}E(X) &= \int_0^{u_m} \sqrt{1 + X_u^2} du + \sigma X(0) + \kappa \int_0^{u_m} uX(u) du - \lambda \left(\int_0^{u_m} X(u) du - V/2 \right) \\ &= \int_0^{u_m} \sqrt{1 + X_u^2} du - \sigma \int_0^{u_m} X_u du + \kappa \int_0^{u_m} uX(u) du - \lambda \left(\int_0^{u_m} X(u) du - V/2 \right) \\ &=: \int_0^{u_m} G du + \lambda V/2 = \int_0^{u_m} G_1(X_u) + G_2(u, X(u)) du + \lambda V/2, \end{aligned}$$

where $G_1 := \sqrt{1 + X_u^2} - \sigma X_u$ and $G_2 := \kappa uX(u) - \lambda X(u)$. First notice the identity

$$(C.4) \quad G - X_u G_{X_u} \Big|_{u_m} = \frac{1}{\sqrt{1 + X_u^2}} \Big|_{u_m} = 0.$$

Then we have

$$\begin{aligned} \frac{1}{2} \frac{d}{ds} \Big|_{s=t} E(\tilde{X}(u(s), s)) &= G|_{u_m} \tilde{u}'_m + \int_0^{u_m} G_X \partial_t \tilde{X} + G_{X_u} \partial_u (\partial_t \tilde{X}) du - \lambda'(t) \left(\int_0^{u_m} X(u) du - V/2 \right) \\ &= G|_{u_m} \tilde{u}'_m + \int_0^{u_m} \left(G_X - \frac{d}{du} G_{X_u} \right) \partial_t \tilde{X} du + G_{X_u} \partial_t \tilde{X} \Big|_0^{u_m} - \lambda'(t) \left(\int_0^{u_m} X(u) du - V/2 \right) \\ &= (G - X_u G_{X_u}) \Big|_{u_m} \tilde{u}'_m + \int_0^{u_m} \left(G_X - \frac{d}{du} G_{X_u} \right) \partial_t \tilde{X} du \\ &\quad - G_{X_u} \partial_t \tilde{X} \Big|_{u=0} - \lambda'(t) \left(\int_0^{u_m} X(u) du - V/2 \right) \\ &= \int_0^{u_m} \left(G_X - \frac{d}{du} G_{X_u} \right) \partial_t \tilde{X} du - G_{X_u} \partial_t \tilde{X} \Big|_{u=0} - \lambda'(t) \left(\int_0^{u_m} X(u) du - V/2 \right), \end{aligned}$$

where we used (C.4). Then we introduce the Riemannian metrics

$$(C.5) \quad g_{X(t)}(\partial_t \tilde{X}, \partial_t X) := \partial_t X(0) \partial_t \tilde{X}(0) + \beta \int_0^{u_m} \frac{\partial_t X \partial_t \tilde{X}}{\sqrt{1 + X_u^2}} du.$$

Then the gradient flow of E on manifold \mathcal{M} with respect to the metrics $g_{X(t)}$ is

$$(C.6) \quad \begin{aligned} \beta \frac{\partial_t X}{\sqrt{1 + X_u^2}} &= -G_X + \frac{d}{du} G_{X_u} = \partial_u \left(\frac{X_u}{\sqrt{1 + X_u^2}} \right) - \kappa u + \lambda, \\ X(u_m) &= 0, \quad X_u(u_m) = -\infty, \\ \partial_t X(0, t) &= G_{X_u} = \frac{X_u}{\sqrt{1 + X_u^2}} \Big|_{u=0} - \sigma, \\ &\int_0^{u_m} X(u) du = V/2. \end{aligned}$$

Remark 6. Consider the free energy in 3D

$$(C.7) \quad \frac{E}{2\pi} = \int_0^{u_m} R\sqrt{1+R_u^2} du + \frac{\sigma}{2}R(0)^2 + \frac{\kappa}{2} \int_0^{u_m} uR^2(u) du - \lambda \left(\int_0^{u_m} \frac{1}{2}R(u)^2 du - \frac{V}{2\pi} \right).$$

First, we calculate the first variation of $E_1 := \int_0^{u_m} R\sqrt{1+R_u^2} du$ using the relation

$$\partial_t \tilde{R} = -R_u \partial_t \tilde{u}_m, \quad \text{for } u = u_m.$$

$$\begin{aligned} & \frac{d}{ds} \Big|_{s=t} E_1(\tilde{R}(u(s), s)) \\ &= R\sqrt{1+R_u^2} \Big|_{u_m} \tilde{u}'_m + \int_0^{u_m} \sqrt{1+R_u^2} \partial_t \tilde{R} + \frac{RR_u}{\sqrt{1+R_u^2}} \partial_t \tilde{R}_u du \\ &= R\sqrt{1+R_u^2} \Big|_{u_m} \tilde{u}'_m + \int_0^{u_m} \sqrt{1+R_u^2} \partial_t \tilde{R} - \partial_u \left(\frac{RR_u}{\sqrt{1+R_u^2}} \right) \partial_t \tilde{R} du + \frac{RR_u}{\sqrt{1+R_u^2}} \partial_t \tilde{R} \Big|_0^{u_m} \\ &= R \left(\sqrt{1+R_u^2} - \frac{R_u^2}{\sqrt{1+R_u^2}} \right) \Big|_{u_m} \tilde{u}'_m + \int_0^{u_m} \sqrt{1+R_u^2} \partial_t \tilde{R} - \partial_u \left(\frac{RR_u}{\sqrt{1+R_u^2}} \right) \partial_t \tilde{R} du - \frac{RR_u}{\sqrt{1+R_u^2}} \partial_t \tilde{R} \Big|_{u=0} \\ &= \int_0^{u_m} \left[\sqrt{1+R_u^2} - \partial_u \left(\frac{RR_u}{\sqrt{1+R_u^2}} \right) \right] \partial_t \tilde{R} du - \frac{RR_u}{\sqrt{1+R_u^2}} \partial_t \tilde{R} \Big|_{u=0}, \end{aligned}$$

where we used $\left(\sqrt{1+R_u^2} - \frac{R_u^2}{\sqrt{1+R_u^2}} \right) \Big|_{u_m} = \frac{1}{\sqrt{1+R_u^2}} \Big|_{u_m} = 0$.

Second, we calculate the first variation of $E_2 := \frac{\sigma}{2}R(0)^2 + \frac{\kappa}{2} \int_0^{u_m} uR^2(u) du - \lambda \left(\int_0^{u_m} \frac{1}{2}R(u)^2 du - \frac{V}{2\pi} \right)$.

$$\begin{aligned} & \frac{d}{ds} \Big|_{s=t} E_2(\tilde{R}(u(s), s)) \\ &= \sigma R(0) \partial_t \tilde{R}(0) + \int_0^{u_m} \kappa u R \partial_t \tilde{R} - \lambda R \partial_t \tilde{R} du - \tilde{\lambda}' \left(\int_0^{u_m} \frac{1}{2} R(u)^2 du - \frac{V}{2\pi} \right). \end{aligned}$$

Therefore, the gradient flow

$$(C.8) \quad g_{R(t)}(\partial_t \tilde{R}, \partial_t R) := R(0) \partial_t R(0) \partial_t \tilde{R}(0) + \beta \int_0^{u_m} \frac{\partial_t R \partial_t \tilde{R}}{\sqrt{1+R_u^2}} R du = -\frac{1}{2\pi} \frac{d}{ds} \Big|_{s=t} E(\tilde{R}(u(s), s))$$

gives the governing equation in 3D

$$(C.9) \quad \begin{aligned} \beta \frac{\partial_t R}{\sqrt{1+R_u^2}} &= -\frac{\sqrt{1+R_u^2}}{R} + \frac{1}{R} \partial_u \left(\frac{RR_u}{\sqrt{1+R_u^2}} \right) - \kappa u + \lambda, \\ \partial_t R(0) &= - \left(\sigma - \frac{R_u}{\sqrt{1+R_u^2}} \Big|_{u=0} \right) = -(\sigma + \cos \theta), \\ V &= \int_0^{u_m} \pi R^2 du, \end{aligned}$$

where θ is defined as $\tan \theta = -R_u|_{u=0}$.

Notice

$$(C.10) \quad \frac{\sqrt{1+R_u^2}}{R} - \frac{1}{R} \partial_u \left(\frac{RR_u}{\sqrt{1+R_u^2}} \right) = \frac{1}{R\sqrt{1+R_u^2}} - \frac{R_{uu}}{(1+R_u^2)^{3/2}},$$

which is the curvature in terms of $R(u)$.

C.1.1. *Desingularized DAEs for quasi-static dynamics of a non-wetting droplet.* Now we derive the desingularized DAEs for the quasi-static dynamics of a non-wetting droplet, which is similar to the partially wetting case. Assume $\beta = 0$ in (C.6). Notice $\frac{X_u}{\sqrt{1+X_u^2}}\Big|_{u=0} = \frac{1}{\sqrt{1+\tan^2\theta(t)}} = -\cos\theta(t)$. The quasi-static dynamics becomes (4.39).

Instead of $X_u(u_m) = -\infty$, to desingularize X_u , we propose an alternative boundary condition use the volume preserving condition. From

$$(C.11) \quad \frac{V}{2} = \int_0^{u_m} \frac{du}{du} X(u) du = - \int_0^{u_m} u X_u du,$$

we have

$$(C.12) \quad u_m X(0) - \frac{V}{2} = \int_0^{u_m} (u - u_m) X_u du.$$

Thus the boundary condition $X_u(u_m) = -\infty$ can be replaced by the nonlocal Dirichlet boundary condition

$$(C.13) \quad X(0, \cdot) = \frac{V}{2u_m} + \frac{1}{u_m} \int_0^{u_m} (u - u_m) X_u du.$$

Integrating once in the first equation of (4.39), we have

$$(C.14) \quad \frac{X_u}{\sqrt{1+X_u^2}} = \frac{\kappa u^2}{2} - \lambda u - \cos\theta,$$

where we used $\frac{X_u}{\sqrt{1+X_u^2}}\Big|_{u=0} = -\cos\theta$ and $\theta = \theta(t)$ depends only on t . Recall the notation in (4.8). Denote

$$(C.15) \quad J(u, \theta) := -\frac{\kappa u^2}{2} + \lambda u + \cos\theta.$$

From the boundary condition $X_u(u_m) = -\infty$ we know

$$(C.16) \quad J(u_m, \theta) = -\frac{\kappa u_m^2}{2} + \lambda u_m + \cos\theta = 1.$$

In fact, when $\kappa < 0, \lambda > 0$, we know there is a unique u_m such that $J(u_m, \theta) = 1$. Then we have

$$(C.17) \quad \frac{dX}{du} = \frac{-J(u, \theta)}{\sqrt{1 - J(u, \theta)^2}}, \quad 0 \leq u \leq u_m,$$

and (C.13) can be recast as

$$(C.18) \quad X(0, \cdot) = \frac{V}{2u_m} + \frac{1}{u_m} \int_0^{u_m} (u - u_m) \frac{-J(u, \theta)}{\sqrt{1 - J(u, \theta)^2}} du.$$

To formulate a complete DAEs, we use another desingularized formula for the volume constraint. Denote $w^2 = u_m - u$, then (C.11) becomes

$$(C.19) \quad \frac{V}{2} = \int_0^{u_m} u X_u du = \int_0^{\sqrt{u_m}} \frac{-2uJ(u, \theta)}{\sqrt{1 + J(u, \theta)}} \frac{\sqrt{u_m - u}}{\sqrt{1 - J(u, \theta)}} dw.$$

By L'Hospital's law, $\lim_{u \rightarrow u_m} \frac{u_m - u}{1 - J(u)} = \lim_{u \rightarrow u_m} \frac{-1}{\kappa u - \lambda} \neq 0$ provided $\kappa u_m \neq \lambda$. Therefore we obtain the DAEs for $(X(0, t), u_m(t), \theta(t), \lambda(t))$ (4.40).

APPENDIX D. CONSTRUCTED BREATHING DROPLET WITH CLOSED FORMULA IN 3D

In this section we give the breathing droplet solution with closed formula in 3D.

Step 1. Given the initial data $\theta(0)$ and $b(0)$. Calculate volume V from (4.23).

Step 2. Calculate $u(r, t)$ and $b(t)$. From the spherical cap formula (4.23)

$$(D.1) \quad b(t)^3 = \frac{3V \sin^3 \theta}{\pi(2 - 3 \cos \theta + \cos^3 \theta)},$$

and from $R(t) = \frac{b(t)}{\sin \theta(t)}$, $R(t) - u_m(t) = R \cos \theta(t)$ we have

$$(D.2) \quad u(r, t) = -R(t) \cos \theta(t) + \sqrt{R(t)^2 - r^2}, \quad x \in (-b(t), b(t)).$$

This construction automatically preserves the volume V and we know

$$(D.3) \quad \sqrt{1 + (u_r)^2} = \frac{R(t)}{\sqrt{R(t)^2 - r^2}}, \quad H = -\nabla \cdot \left(\frac{\nabla u}{\sqrt{1 + |\nabla u|^2}} \right) = -\frac{1}{r} \partial_r \left(\frac{r \partial_r u}{\sqrt{1 + (\partial_r u)^2}} \right) = \frac{2}{R(t)}.$$

Step 3. We find $\kappa(t), \sigma(t)$ and $\lambda(t)$ such that

$$(D.4) \quad \beta \frac{\partial_t u(r, t)}{\sqrt{1 + (\partial_r u)^2}} = -H - \kappa(t)u + \lambda(t), \quad r \in (0, b(t)),$$

$$b'(t) = -\sigma(t) - \frac{1}{\sqrt{1 + (\partial_r u)^2}}, \quad r = b(t).$$

From the formula in Step 2, we can solve

$$\kappa(t) = -\beta \cos \theta \left(1 + \frac{1}{3}(\cot^2 \theta + \frac{\pi b^3}{V \sin \theta}) \right) \dot{\theta},$$

$$\lambda(t) = \frac{2}{R} + \beta R \cos \theta \dot{\theta} + \frac{\beta R}{3}(\cos \theta - \tan \theta)(\cot^2 \theta + \frac{\pi b^3}{V \sin \theta}) \dot{\theta},$$

$$\sigma(t) = \frac{b}{3}(\cot \theta - \frac{\pi}{V} b^3) \dot{\theta} - \cos \theta(t).$$

Particularly, for the quasi-static case $\beta = 0$, we have

$$(D.5) \quad \kappa(t) = 0, \quad \lambda(t) = \frac{2}{R(t)}.$$